Discovery of BUB1 kinase inhibitors for the treatment of cancer

Bosman, R.E.J.

2

Discovery of novel BUB1 inhibitors by high-throughput screening

Introduction

Breast cancer is the most common cancer among women worldwide, with an estimated 2.2 million new cases in 2020.[1] In addition, breast cancer was the leading cause of cancer related deaths among women in 2020.[1] There are three main subtypes of breast cancer and assessment of breast cancer subtype is predominantly based on the expression of the estrogen receptor alpha (ERα), progesterone receptor (PR) and human epidermal growth factor receptor 2 (HER2).[2] Clinical decisions for breast cancer therapy rely on the expression of these receptors and breast cancer subtypes therefore include: hormone receptor positive/HER2 negative ($HR^+/HER2^-$), HER2 positive ($HER2^+$) and triple-negative.[3] The $HR^+/HER2^-$ subtype, which represents the majority of the patient group (~73%)[4], is treated with endocrine therapy. Endocrine therapy counteracts estrogen-promoted tumor growth by, for example, tamoxifen, which is an ER modulator[5], or by aromatase inhibitors (i.e. anastrozole, exemestane, letrozole), which decrease estrogen levels.[6] $HR^+/HER2^-$ breast cancers showing high expression of ER and PR are usually of lower grade, show low proliferation rates and therefore have good prognosis.[7] $HER2^+$ tumors (~15%)[4], which can either be HR^+ or HR^-, have intermediate prognosis[7] and are treated with a combination of chemotherapy and HER2-targeted therapies.[3] Chemotherapy includes DNA binding drugs, such as doxorubicin, cyclophosphamide or carboplatin, or microtubule targeting drugs, such as taxanes (i.e. docetaxel, paclitaxel). HER2 can be targeted by anti-HER2 antibodies, such as trastuzumab or pertuzumab.[8] Alternatively, the intracellular kinase domain of HER2 can be inhibited by small molecule inhibitors like lapatinib and neratinib, thereby inhibiting downstream signal transduction.[9] $HER2^+$ tumors that stain positive for hormone receptors may also be treated with endocrine therapy. Triple-negative breast cancer (TNBC), which accounts for ~12% of all breast cancers[4], shows high proliferation and has poor prognosis.[7] TNBC is characterized by the lack of expression of both hormone receptors as well as HER2 expression, which limits therapeutic options to only general chemotherapy due to the lack of a molecular target. Therefore, new treatments for TNBC based on novel molecular targets are urgently needed. Targeting kinases of the spindle assembly checkpoint has emerged as a potential strategy.[10–12]

The spindle assembly checkpoint (SAC) is a safety mechanism during mitosis which prevents mitotic progression when chromosomes are not correctly attached to the mitotic spindle.[13] The SAC is active during the prometaphase of mitosis and prevents anaphase initiation by inhibiting the anaphase-promoting complex/cyclosome (APC/C).[13] SAC signaling involves a multitude of proteins, including kinases such as BUB1. Many cancer cells suffer from a diminished SAC and interference with these weakened checkpoints is thought to cause severe chromosomal instability which eventually results in cell death.[10,11] Targeting kinases of the SAC by small molecule inhibitors has therefore emerged as a new strategy to kill cancer cells.

BUB1 fulfills important roles in the SAC by recruiting numerous of proteins to kinetochores which are important for SAC signaling.[14–17] The importance of the kinase function of BUB1, however, has been subject of debate.[18–20] Until recently, no optimized BUB1 inhibitors had been published, which hindered the investigation of the kinase function of BUB1 in cancer cell proliferation. In 2019, Siemeister *et al.*[12] published the first optimized BUB1 inhibitor, BAY1816032 (**Figure 2.1**), which was based on their earlier report from Baron *et al.*[21] BAY1816032 was evaluated *in vivo* using a human TNBC mouse xenograft model and synergistically inhibited tumor growth when combined with paclitaxel.[12] Tumor growth inhibition with this combined treatment outperformed the efficacy of treatment with paclitaxel alone. However, BAY1816032 did not show efficacy as single agent. The reason for this lack of efficacy remains unclear, but might be due to incomplete BUB1 inhibition. Recently, it was suggested that about 4% of BUB1 levels remain after CRISPR/Cas9-mediated BUB1 knockout and this amount was hypothesized to be sufficient for normal SAC activity.[22] Therefore, more potent BUB1 inhibitors are required.

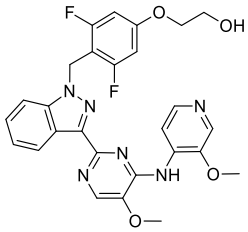

Figure 2.1 | Chemical structure of BUB1 inhibitor BAY1816032.

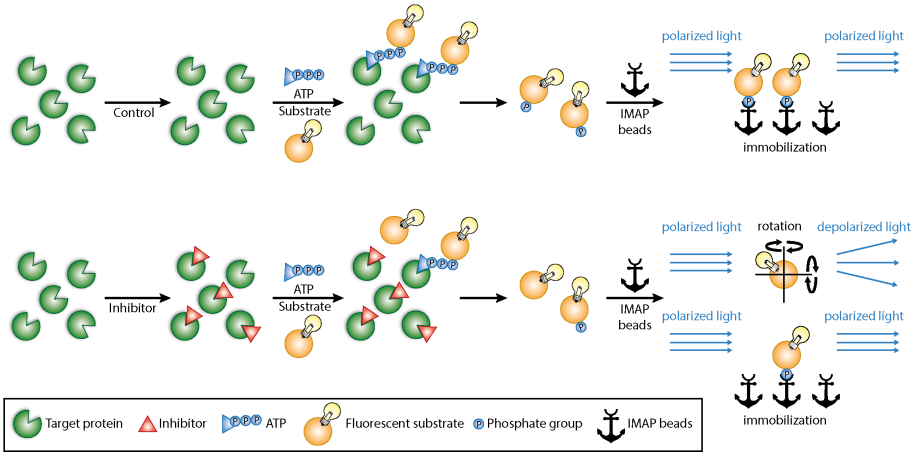

Figure 2.2 | Schematic representation of the fluorescence polarization assay to measure the kinase activity of BUB1. Control samples (top) are incubated with ATP and a fluorescent peptide substrate that can be phosphorylated by BUB1. Addition of IMAP (immobilized metal affinity for phosphochemicals) beads[23] causes immobilization of the phosphorylated substrate fraction. Immobilization of the fluorescent substrate reduces its rotational speed and thereby retaining the polarized light. For inhibitor treated samples (bottom), only a fraction of the peptide substrate is phosphorylated. The unphosphorylated fraction remains free in solution and due to its rotational freedom, depolarization of the light occurs. Depolarization of the light is therefore related to inhibitor potency.

In this chapter, the results of a high-throughput screen (HTS)[24,25], using a fluorescence polarization assay[26,27] (**Figure 2.2**), to identify new chemotypes as BUB1 inhibitors are described (see **Box 2.1** for alternative hit identification strategies). A hit list of 25 molecules was obtained and resynthesis of four prioritized hits resulted in the confirmation of their activity.

Box 2.1 | Hit identification

In drug discovery, target selection (**Chapter 1**) is followed by hit identification. Several hit identification strategies can provide the basis for a drug discovery program, such as selective optimization of side activities (SOSA) of drug molecules[28], fragment-based drug discovery (FBDD)[29], virtual screening[30] or high-throughput screening.[24,25] SOSA is based on the observation that approved drugs might suffer from one or several pharmacological side effects due to binding of the drug with unintended protein targets. These off-target activities can be used as starting point for drug discovery for a new biological target. In FBDD a relatively small library (~1000 compounds) of diverse molecules with low molecular weights (typically 100 – 250 Da) is screened on purified kinases.[29] This results in inhibitors with low binding affinities (μM – mM range), but with high ligand efficiencies[31], a metric that describes the average binding energy per atom. Sensitive screening technologies are required for FBDD as well as significant amounts of purified protein. Virtual screening can be categorized into two major approaches: ligand-based screening and structure-based screening.[30] For ligand-based screening known active molecules are used to build pharmacophore models or are transformed into molecular fingerprints. Screening a virtual molecular library in these models or similarity searches using the fingerprints may yield novel hits. Structure-based screening can be performed in case three-dimensional structural information of the protein of interest is available. High-throughput screening (HTS)[24,25] is an automated way of screening large compound libraries (~10^4 – 10^6 molecules) which include historical compound collections, natural products and/or combinatorial chemistry libraries.[32] Initiating a HTS campaign requires an assay that can distinguish active compounds from inactive ones. These assays have to be miniaturized, usually in 384- or 1536-well plates, to save reagents and compounds, thereby reducing costs.

Results & Discussion

High-throughput screen

High-throughput screening was performed at the Pivot Park Screening Centre (PPSC) (Oss, The Netherlands). A fluorescence polarization assay was miniaturized from a 384- to a 1536-well plate format. A library, enriched with kinase inhibitors and consisting of 53,408 compounds, was screened at a concentration of 10 μM. The quality of the data throughout the screening campaign was evaluated by monitoring the Z′-factor[33] and assay window (in ΔmP) for each assay plate. Active compounds (actives) were distinguished by Z-scores[34] for which Z-score < –4 was used as cutoff. For the primary screen, Z′-factor ≥ 0.67 and ΔmP ≥ 91 were obtained (**Supplementary Figure 1**, p. 46), indicating good quality. The complete library was screened in one day, after which 704 primary actives were found (~13% effect) (**Figure 2.3A,C**). All primary actives were screened again at a concentration of 10 μM, which resulted in 214 confirmed actives (Z′-factor ≥ 0.57 and ΔmP ≥ 99) (**Figure 2.3B,C**). These compounds were investigated for potential interference with the fluorescence polarization assay by applying a different experimental setup. Briefly, BUB1 was mixed with ATP and

fluorescent peptide substrate to allow for maximum phosphorylation of the peptide substrate. Instead of pre-incubating BUB1 with the compounds, compounds were added at this stage. Compounds that still decreased polarization of light, interfered with the assay and were therefore deselected. In total, 57 compounds were found to interfere with the assay (Z-score < –4, Z'-factor ≥ 0.69 and ΔmP ≥ 102). Of the remaining 157 compounds, 74 molecules were selected and dose-response curves were determined. Based on potency, the shape of the IC_{50} curves, drug-likeness (molecular weight <450 g/mol and logP <4 (with a few exceptions for compounds with favorable potency)) and removal of pan-assay interference compounds (PAINS), a hit list of compounds (**1** – **25**) was obtained (**Table 2.1**). Purity and molecular weight of these compounds were confirmed by liquid chromatography-mass spectrometry (LCMS) analysis.

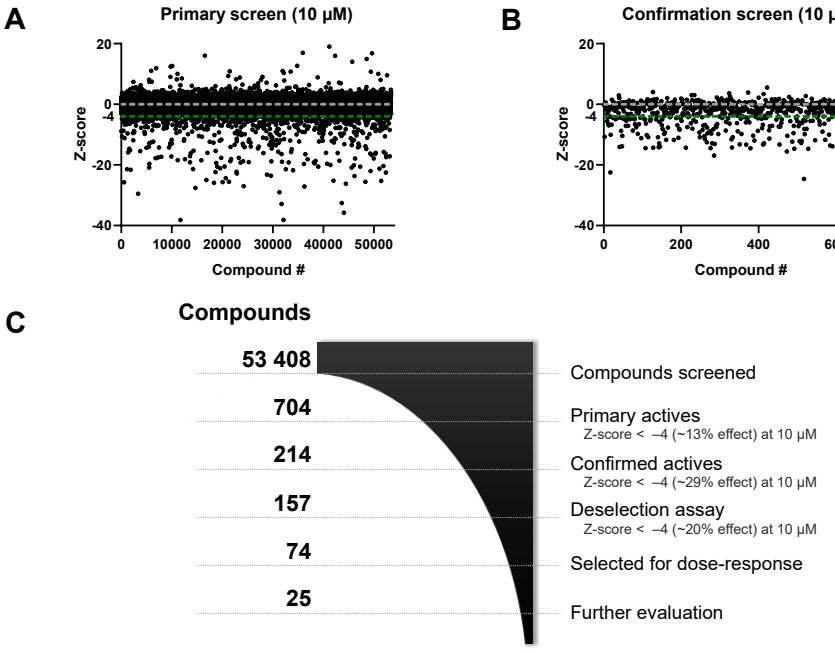

Figure 2.3 | Summary of the high-throughput screen. (A) Z-scores obtained from the primary screen. Z-score < –4 was used as cutoff for primary actives. **(B)** Z-scores obtained from the confirmation screen. Z-score < –4 was used as cutoff for confirmed actives. **(C)** Summary of the high-throughput screen.

Table 2.1 | Qualified hit list and corresponding physicochemical parameters.

ID	Name[a]	Structure	pIC_{50}[b]	App. K_i (nM)[c]	MW[d]	LE[e]	cLogP[f]	LipE[g]	Ref.[h]
1	AT-9283	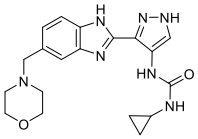	6.78	103	381	0.34	0.4	6.5	[35]
2	CYC-116	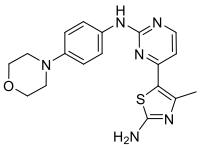	6.75	110	368	0.37	3.0	4.0	[36]
3	OSI-420	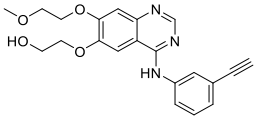	6.59	159	379	0.33	2.6	4.2	[37]
4	PP-121	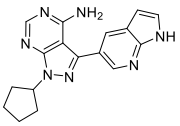	6.32	296	319	0.37	2.0	4.5	[38]
5	PF-00477736	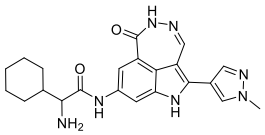	6.51	191	419	0.30	0.9	5.8	[39,40]
6	Ralimetinib (LY-2228820)	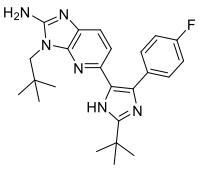	6.17	419	421	0.28	5.2	1.2	[41]
7	Momelotinib (CYT-387)	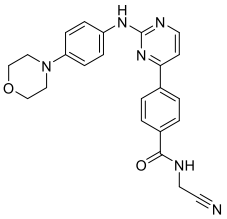	6.10	492	414	0.28	2.5	3.8	[42,43]
8	BCC0044301	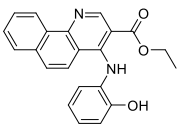	6.04	565	358	0.32	4.7	1.6	–
9	Erlotinib	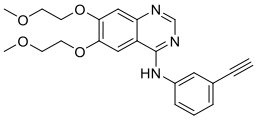	5.79	1004	393	0.28	3.1	2.9	[44,45]

Table 2.1 | Qualified hit list and corresponding physicochemical parameters (continued).

ID	Name[a]	Structure	pIC_{50}[b]	App. K_i (nM)[c]	MW[d]	LE[e]	cLogP[f]	LipE[g]	Ref.[h]
10	NP_000412	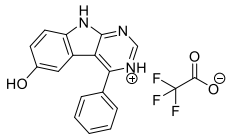	5.65	1386	261	0.40	3.1	2.7	[46,47]
11	BCC0090688	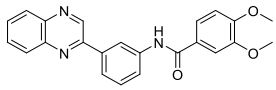	5.58	1629	385	0.27	3.9	1.9	–
12	SPCE000468_01	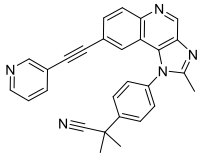	5.53	1827	428	0.24	5.3	0.5	[48]
13	AZD-5438	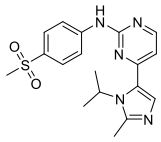	5.44	2248	371	0.30	2.1	3.5	[49]
14	BCC0114359	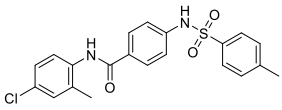	5.42	2354	415	0.28	4.4	1.2	–
15	CP-466722	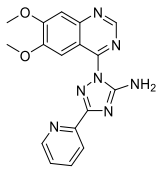	5.41	2409	349	0.30	2.2	3.4	[50,51]
16	SPCE000116_01	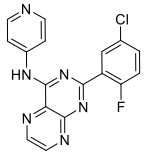	5.41	2409	353	0.31	3.0	2.6	[52]
17	BCC0049010	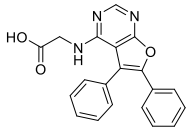	5.39	2522	345	0.30	3.4	2.2	[53]
18	PF-4800567	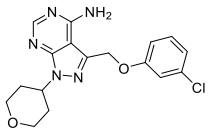	5.31	3033	360	0.30	2.1	3.4	[54]
19	BCC0104036	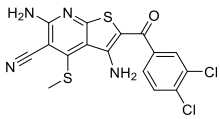	5.21	3818	409	0.30	3.4	2.0	–

Table 2.1 | Qualified hit list and corresponding physicochemical parameters (continued).

ID	Name[a]	Structure	pIC_{50}[b]	App. K_i (nM)[c]	MW[d]	LE[e]	cLogP[f]	LipE[g]	Ref.[h]
20	Reversine	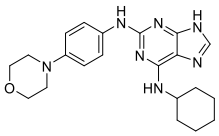	5.20	3907	393	0.26	3.1	2.3	[55]
21	BCC0088074	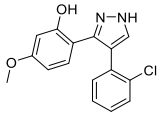	5.17	4186	301	0.35	3.2	2.2	–
22	BCC0075829	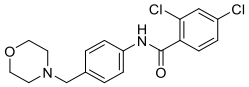	5.16	4284	365	0.31	3.6	1.8	–
23	TWS-119	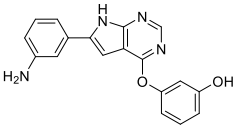	5.08	5150	318	0.30	2.9	2.4	[56,57]
24	Silmitasertib (CX-4945)	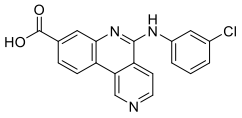	5.06	5393	350	0.29	4.0	1.3	[58]
25	Axitinib (AG-013736)	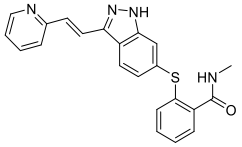	5.03	5778	386	0.26	3.4	1.8	[59,60]

[a] Published compound name or code, otherwise compound code from HTS library; [b] Half maximal inhibitory concentrations (expressed as pIC_{50}) from high-throughput dose-response assay; [c] app. K_i: apparent K_i as determined by the Cheng-Prusoff equation[61]; [d] MW: molecular weight (g/mol); [e] LE: ligand efficiency[31], defined as: $\mathrm{LE} = (-RT * \ln(\mathrm{app.}\,K_i))/\mathrm{HA}$, where HA stands for the number of 'heavy atoms' (non-hydrogen atoms); [f] cLogP: LogP calculated by DataWarrior (v.5.2.1); [g] LipE: lipophilic efficiency[31], defined as: $\mathrm{LipE} = \mathrm{app.}\,pK_i - \mathrm{cLogP}$; [h] reference.

Hit prioritization

The main compound properties considered for hit prioritization included half maximal inhibitory concentrations (pIC_{50}), ligand efficiency (LE, calculated as defined in **Table 2.1**), calculated LogP (cLogP), lipophilic efficiency (LipE, calculated as defined in **Table 2.1**) and molecular weight (MW). Additionally, synthetic accessibility was taken into account as well as the availability of co-crystallized structures with kinases. Hits **8** – **25** have pIC_{50} values below 6 or a high cLogP, which resulted in a low to moderate LipE. Compounds **5** – **7** have a molecular weight above 413 Da, which resulted in a low LE, which is undesirable in view of the fact that MW generally increases during hit optimization.[62] In addition, the synthetic accessibility of hit **5** was deemed low.[63] The remaining hits, **1** – **4**, had an acceptable molecular weight (MW ≤ 381) as well as good activity (pIC_{50} > 6.3), ligand efficiency (LE ≥ 0.33), lipophilicity (cLogP ≤ 3.0) and lipophilic efficiency (LipE ≥ 4.0). In addition, co-crystal

structures with kinases have been published for hits **1**, **2**, **4** as well as for an analogue of compound **3**.[35,36,64,65] Taken together, compounds **1** – **4** were prioritized for hit confirmation. In the following sections a short description of each hit, their resynthesis and biochemical evaluation is described.

Resynthesis of hit 1

The discovery of compound **1** (1-cyclopropyl-3-(3-(5-(morpholinomethyl)-1*H*-benzo[*d*]imidazol-2-yl)-1*H*-pyrazol-4-yl)urea, or AT-9283) was first reported in 2009.[35] AT-9283 (**1**) is a potent inhibitor of multiple kinases including Aurora A, Aurora B, JAK2 and JAK3. In addition, high activities (pIC_{50} > 7) were also reported for over 30 other kinases.[35] AT-9283 (**1**) has been investigated in several phase I clinical trials in patients with leukemia, solid tumors and non-Hodgkin's lymphoma[66–69] and as such may represent an excellent starting point for a new drug discovery program. Synthesis of **1** (AT-9283) was performed by using previously published procedures[35] with minor modifications (**Scheme 2.1**). In short, 3,4-dinitrobenzoic acid was converted into its acyl chloride, followed by a peptide bond formation with morpholine. Amide **26** was reduced to amine **27** of which the nitro groups were subsequently reduced to their corresponding amines to form **28**. A peptide coupling was performed with 4-nitro-1*H*-pyrazole-3-carboxylic acid and subsequent cyclization resulted in benzimidazole **29**. The nitro group of **29** was reduced to amine **30** which was used to form the cyclopropyl urea of AT-9283 (**1**).

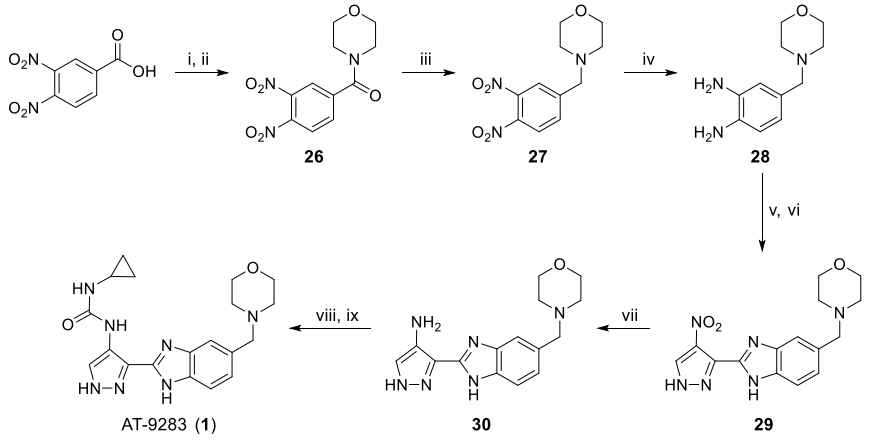

Scheme 2.1 | Synthesis of hit AT-9283. Reagents and conditions: **i)** $SOCl_2$, DMF, THF, 70°C. **ii)** Et_3N, morpholine, 0°C → RT, 93%. **iii)** $NaBH_4$, $BF_3{\cdot}OEt_2$, THF, 0°C → RT, 77%. **iv)** 10% Pd/C, EtOH, 81%. **v)** 4-nitro-1*H*-pyrazole-3-carboxylic acid, EDC·HCl, HOBt, DMF. **vi)** AcOH, 118°C, 55%. **vii)** 10% Pd/C, MeOH, 72%. **viii)** CDI, THF, 66°C. **ix)** cyclopropylamine, DMF, 100°C, 33%.

Resynthesis of hit 2

CYC-116 (**2**), or 4-methyl-5-(2-((4-morpholinophenyl)amino)pyrimidin-4-yl)thiazol-2-amine, was identified by investigation of the structure-activity relationship of a similar compound found through cell-based screens.[36] CYC-116 (**2**) is a potent inhibitor of Aurora A and B with sub-nanomolar activity, inhibited proliferation of multiple cancer cell lines and reduced

tumor growth in several *in vivo* tumor models.[36] The compound was evaluated in phase I clinical trials, however, this study was terminated by the sponsor for unknown reasons.[70] Hit **2** (CYC-116) was synthesized employing previously described procedures (**Scheme 2.2**).[36,71] In brief, 1-fluoro-4-nitrobenzene was used for a nucleophilic aromatic substitution with morpholine to obtain **31**.[72] Palladium catalyzed reduction of the nitro group was performed to form **32**. The amine of **32** was converted into a guanidine under acidic conditions.[73] In parallel, 3-chloropentane-2,4-dione was reacted with thiourea to form thiazole **34**, which was subsequently transformed into enaminone **35** by using DMF-DMA. Guanidine **33** and enaminone **35** were condensed to form a pyrimidine and afforded CYC-116 (**2**).

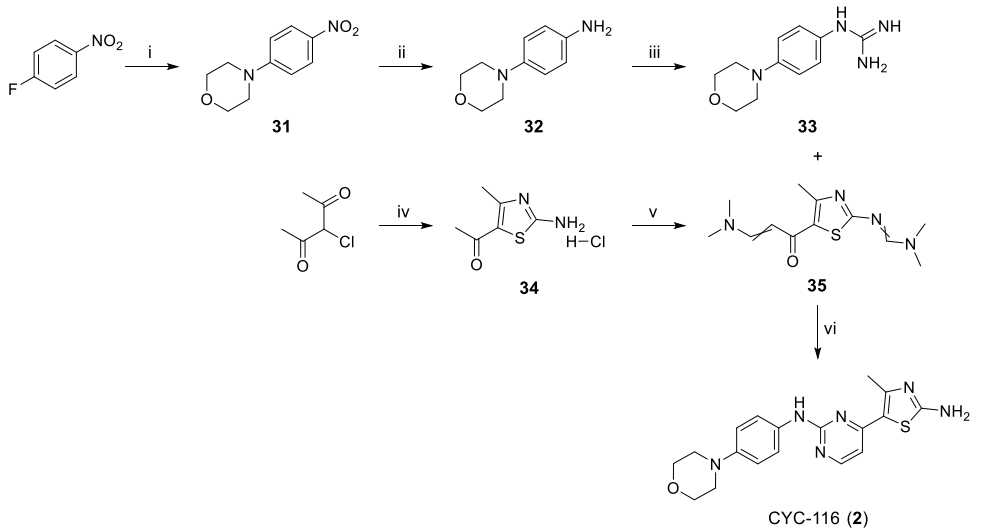

Scheme 2.2 | Synthesis of hit CYC-116. Reagents and conditions: **i)** morpholine, Et_3N, MeCN, 82°C, 93%. **ii)** 10% Pd/C, MeOH, 91%. **iii)** conc. HCl (aq.), cyanamide (aq.), EtOH, 0 → 78°C, 96%. **iv)** thiourea, pyridine, MeOH, 0°C → RT, 89%. **v)** DMF-DMA, 105°C, 70%. **vi)** Na_2CO_3, 2-methoxyethanol, 124°C, 46%.

Resynthesis of hit 3

Compound **3** (2-((4-((3-ethynylphenyl)amino)-7-(2-methoxyethoxy)quinazolin-6-yl)oxy)ethan-1-ol, or OSI-420) is a metabolite of approved drug erlotinib.[37] Erlotinib is an inhibitor of the human epidermal growth factor receptor (EGFR), a membrane receptor tyrosine kinase, and is used in the treatment of non-small cell lung cancer.[74] Interestingly, in addition to OSI-420, erlotinib was identified as one of the hits (**9**) (**Table 2.1**). However, erlotinib (**9**) showed a 6-fold reduced potency, suggesting that the free hydroxyl of OSI-420 (**3**) is an important structural feature for its activity. Hit **3** was synthesized according to published procedures[75–77] (**Scheme 2.3**). Ethyl 3,4-dihydroxybenzoate was subjected to a Mitsunobu reaction with benzyl alcohol to selectively protect the alcohol *para* to the ester (regioselectivity was confirmed by 1H-1H-ROESY NMR).[76] The free alcohol of **36** was subsequently alkylated with 2-bromoethyl acetate, after which the benzyl protecting group was removed and the resulting free alcohol was alkylated with 1-bromo-2-methoxyethane to afford **39**. The nitro group was regioselectively introduced[77] by a Menke nitration to afford

40 (regioselectivity was confirmed by 1H-1H-ROESY NMR). The nitro group was reduced and the obtained free amine was used for a Niementowski reaction to obtain quinazolinone **42**. The quinazolinone was chlorinated to form 4-chloroquinazoline **43** which was used for a nucleophilic aromatic substitution with 3-ethynylaniline to obtain **44**. Deacetylation finally led to the formation of **3**.

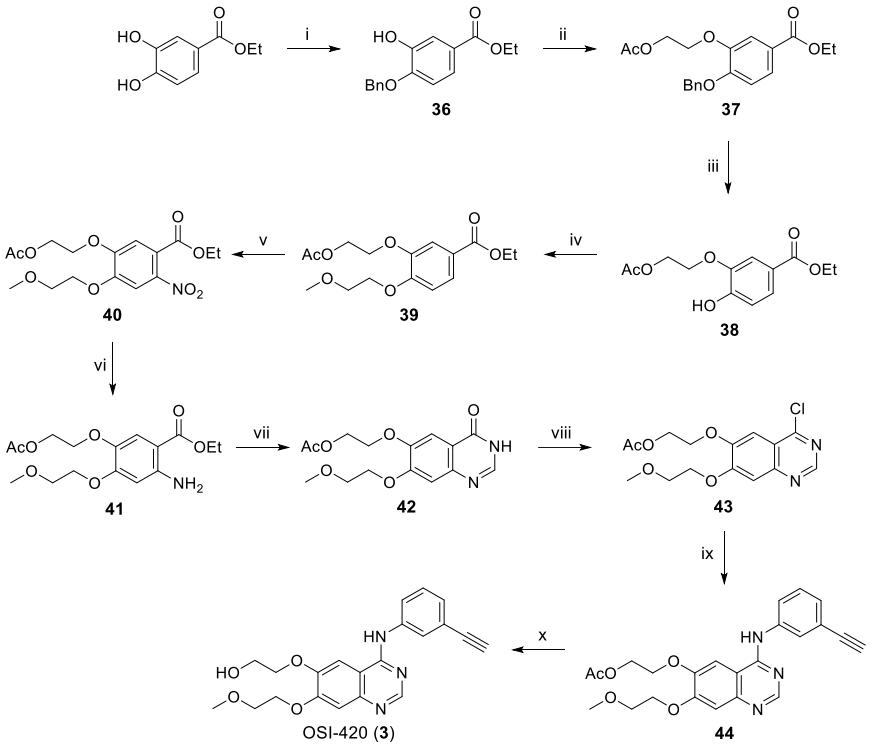

Scheme 2.3 | Synthesis of hit OSI-420. Reagents and conditions: **i)** Ph_3P, DIAD, BnOH, THF, 0°C → RT, 41%. **ii)** 2-bromoethyl acetate, K_2CO_3, DMF, 100°C, 72%. **iii)** 10% Pd/C, MeOH, 98%. **iv)** 1-bromo-2-methoxyethane, K_2CO_3, DMF, 100°C, 96%. **v)** $Cu(NO_3)_2 \cdot 3H_2O$, Ac_2O, 0°C → RT, 73%. **vi)** 5% Pt/C, MeOH, 66%. **vii)** NH_4HCO_2, formamide, 160°C, 60%. **viii)** $POCl_3$, 105°C, 80%. **ix)** 3-ethynylaniline, 2-propanol, 82°C, quant. **x)** 0.4 M NaOH in MeOH, 27%.

Resynthesis of hit 4

Compound **4** (1-cyclopentyl-3-(1*H*-pyrrolo[2,3-*b*]pyridin-5-yl)-1*H*-pyrazolo[3,4-*d*]pyrimidin-4-amine, or PP-121), is a multitargeted kinase inhibitor which inhibits several members of the phosphatidylinositol-3-OH kinase (PI(3)K) family of lipid kinases.[38] In addition, high activities were observed for multiple tyrosine kinases, including ABL, HCK, SRC, VEGFR2 and PDGFR, among others.[38] PP-121 (**4**) was found to inhibit proliferation of several cancer cell lines which was attributed to direct inhibition of oncogenic tyrosine kinases and PI(3)Ks.[38] Compound **4** was synthesized as depicted in **Scheme 2.4** using published procedures.[78] 1*H*-pyrazolo[3,4-*d*]pyrimidin-4-amine was halogenated by using *N*-iodosuccinimide to obtain **45**. The endocyclic amine was alkylated by bromocyclopentane to afford **46**.

Subsequent Suzuki coupling with 7-azaindole-5-boronic acid pinacol ester resulted in the formation of PP-121 (**4**).

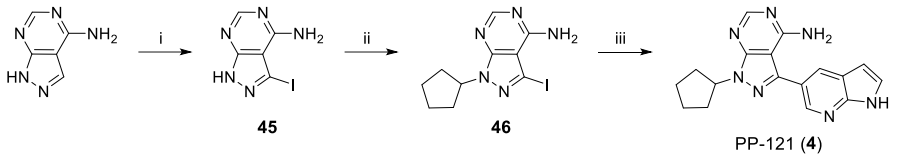

Scheme 2.4 | Synthesis of hit PP-121. Reagents and conditions: **i)** *N*-iodosuccinimide, DMF, 85°C, 63%. **ii)** bromocyclopentane, K_2CO_3, DMF, 80°C, 59%. **iii)** 7-azaindole-5-boronic acid pinacol ester, Na_2CO_3, $Pd(PPh_3)_4$, DMF:H_2O (10:1), 100°C, 70%.

Table 2.2 | Hit confirmation results. Half maximal inhibitory concentrations (expressed as pIC_{50} (± SEM)) and corresponding apparent K_i values from high-throughput screening (HTS) hits and resynthesized hits determined by a biochemical fluorescence polarization assay on BUB1 kinase activity.

ID	Name	pIC_{50} (HTS)	App. K_i (nM)	pIC_{50} ± SEM	App. K_i (nM)
1	AT-9283	6.78	103	6.66 ± 0.02	77
2	CYC-116	6.75	110	6.34 ± 0.05	162
3	OSI-420	6.59	159	6.28 ± 0.05	185
4	PP-121	6.32	296	6.22 ± 0.05	214

Resynthesized hits **1** – **4** were evaluated in the fluorescence polarization assay and observed activities correspond with the potencies obtained from the high-throughput screen (Table 2.2).

Conclusion

High-throughput screening was successfully used to screen over 50,000 compounds and led to the identification of 25 novel BUB1 inhibitors with pIC_{50} values ranging from 5.03 – 6.78. Based on potency and physicochemical properties, hits **1** – **4** were prioritized and subsequently resynthesized. Biochemical evaluation confirmed their activity and these hits, therefore, provide excellent starting points for drug discovery of BUB1 inhibitors. The binding modes of hit **1**, **2**, **4** and the analogue of compound **3** (erlotinib (**9**)) (Figure 2.4) revealed that the cyclopropyl urea of **1**, the aminothiazole of **2**, the phenylacetylene of **3** and azaindole of **4** provide opportunities to reach back pockets of their respective kinases.[35,36,64,65] Since occupation of kinase back pockets contributes to selectivity of inhibitors[79,80] and assuming that these inhibitors may bind similarly in BUB1, modifications of hits **1** – **4** may therefore be aimed at aforementioned part of their structure. For the modification of these groups, reactions with an amino pyrazole (compound **30**, Scheme 2.1) or a chloroquinazoline (compound **43**, Scheme 2.3) were favored over the condensation reaction between compound **33** and **35** (Scheme 2.2) and the Suzuki coupling with **46** (Scheme 2.4). Hit **1** and **3** were therefore selected for hit optimization which will be described in Chapters 4 and 3, respectively.

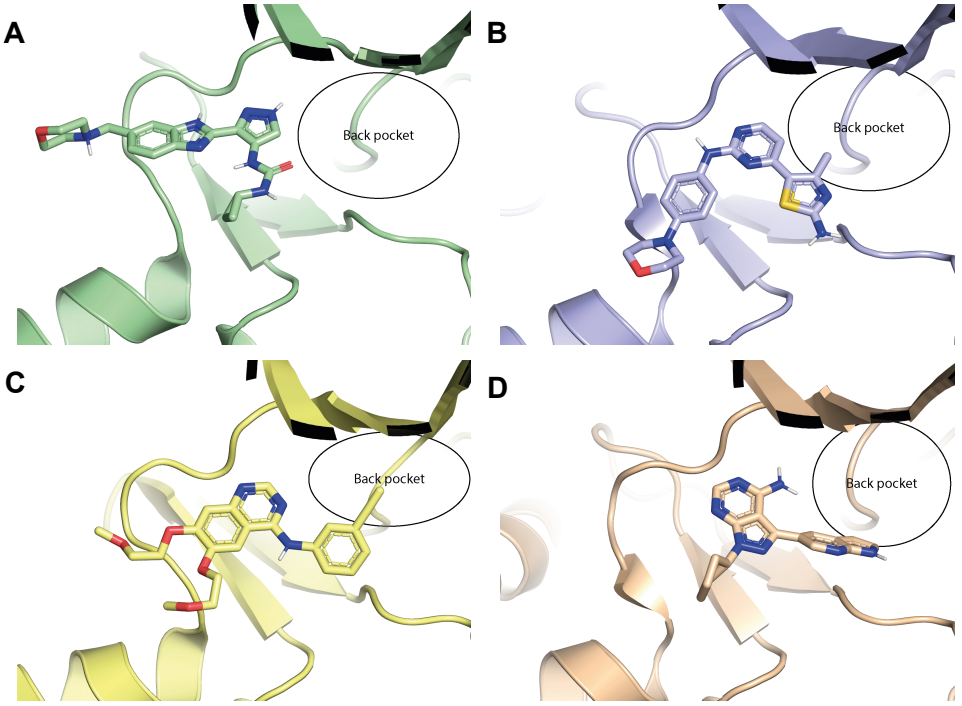

Figure 2.4 | Crystal structures of hits 1, 2, 9 and 4. Crystal structures of **(A)** AT-9283 (**1**) in Aurora A (PDB code: 2W1G)[35], **(B)** CYC-116 (**2**) in CDK2/cyclin A (PDB code: 2UUE)[36], **(C)** Erlotinib (**9**) in EGFR (PDB code: 1M17)[65] and **(D)** PP-121 (**4**) in STK24 (PDB code: 4QMW)[64]. Figures were generated using PyMOL.[81]

Acknowledgements

From Netherlands Translational Research Center (NTRC), Martine Prinsen is kindly acknowledged for the development of the fluorescence polarization assay to measure BUB1 kinase activity and Rogier Buijsman for supervision. Willemijn Wouters, Helma Rutjes and Stan van Boeckel from the Pivot Park Screening Centre (PPSC) are kindly acknowledged for assay miniaturization and conducting the high-throughput screen. Titia Rixt Oppewal is kindly acknowledged for her contribution on AT-9283 (**1**) resynthesis, Julian Clijncke for resynthesizing OSI-420 (**3**) and confirming its activity, and Hans van den Elst for measuring HRMS.

Experimental – Biochemistry

High-throughput screening

All assays were performed in 1536-well plates (Corning, black polystyrene not treated microplate). The primary screen and active confirmation assay were performed by sequential addition (indicated as: volume, final assay concentration, x working solution) of compound (5 or 10 nL, 10 µM, as 400x or 200x working solutions, respectively), BUB1/BUB3 (1 µL, 27 nM, as 2x working solution, Carna Biosciences (05-187), lot: 16CBS-0204) and a mixture of ATP and BUB1/BUB3 substrate (Carna Biosciences (05-187MS-C11)) (1 µL, 5 µM ATP/100 nM substrate, as 2x working solution). Assay reactions were stopped by addition of IMAP progressive binding reagent (2 µL, 1200x diluted (see below), as 2x working solution, Molecular Devices (R7284)).

For each assay, assay buffer (AB) was freshly prepared and consisted of 20 mM HEPES (prepared by diluting 200 mM HEPES, pH 7.4), 5 mM $MgCl_2$, 0.01% (v/v) Tween-20 and 2 mM L-cysteine. Stocks of compounds (in DMSO) were added to the assay plate by using an Echo Liquid Handler. For controls, DMSO was added instead. BUB1/BUB3 (5 µM in storage buffer) was diluted in AB to obtain 54 nM of which 1 µL was added to the assay plate by using a Certus dispenser. For controls, 1 µL of AB was added instead. The assay plate was centrifuged (1 min, 200 *g*) and incubated at RT for 30 min. ATP (40 mM in MilliQ) and BUB1/BUB3 substrate (1 mM) were diluted in AB such to obtain a solution of 10 µM ATP and 200 nM BUB1/BUB3 substrate of which 1 µL was added to each well of the assay plate. The assay plate was centrifuged (1 min, 200 *g*) and incubated at RT in the dark for 120 min. IMAP progressive binding buffer A (5x) and IMAP progressive binding buffer B (5x) were mixed in a ratio to obtain 30% buffer A and 70% buffer B, which was subsequently diluted 5x in MilliQ. IMAP progressive binding reagent was diluted 600x in aforementioned mixture of buffer A and B (to obtain a 2x working solution) of which 2 µL was added to each well of the assay plate. The assay plate was centrifuged (1 min, 200 *g*) and incubated at RT in the dark for 60 min. Fluorescence polarization was measured on an EnVision plate reader (excitation FITC FP 480, 1st emission FITC FP P-pol 535, 2nd emission FITC FP S-pol 535). ActivityBase (IDBS) software was used to analyze data and to calculate quality parameters (Z'-factor and ΔmP). For the deselection assay, in a tube, BUB1/BUB3 (or AB) was first incubated with the mixture of ATP and BUB1/BUB3 substrate for 120 min in the dark. 30 min prior to the end of the incubation time, compounds (or DMSO) were added to an assay plate and aforementioned solution of IMAP progressive binding reagent (2 µL) was added. The assay plate was centrifuged (1 min, 200 *g*) and incubated at RT for 30 min. Subsequently, 2 µL of the mixture of BUB1/BUB3 (or AB), ATP and BUB1/BUB3 substrate (after incubation of 120 min) was added to corresponding wells. The assay plate was centrifuged (1 min, 200 *g*), incubated at RT in the dark for 60 min and fluorescence polarization was measured. For the dose-response assay, stock solutions of compounds (in DMSO) were serially diluted ($\sqrt{10}$ dilutions) in DMSO obtain 10 concentrations (final concentrations of 6.32 nM – 20 µM) as 100x working solutions. 20 nL of compound (or DMSO) was added to the assay plate after which the protocol of the primary screen was followed. ActivityBase was used to calculate pIC_{50} values using the four parameter fitting protocol.

Biochemical evaluation of BUB1 inhibitors

Assays were performed in 384-well plates (Greiner, black, flat bottom, 781076) by sequential addition (indicated as: volume, final assay concentration) of inhibitor (5 µL, 3 nM – 10 µM), BUB1/BUB3 (5 µL, 3.26 nM, Carna Biosciences (05-187), lot: 15CBS-0644 D), ATP (5 µL, 15 µM) and BUB1/BUB3 substrate (5 µL, 75 nM, Carna Biosciences (05-187MSSU)), all as 4x working solutions. The final concentration of DMSO was 1%. Assay reactions were stopped by addition of IMAP progressive binding reagent (20 µL, 1200x diluted (see below), Molecular Devices (R8155), lot: 3117896). Each assay included the following controls: (i) a background control (treated with vehicle instead of inhibitor and BUB1/BUB3 substrate), (ii) MIN controls (treated with 5 µM BAY1816032 (MedChem Express) as inhibitor, defined as 0% BUB1 activity) and (iii) MAX controls (treated with vehicle instead of inhibitor, defined as 100% BUB1 activity). All inhibitors were tested in two separate assays and all inhibitor concentrations were tested in duplicate per assay (N=2, n=2).

For each assay, assay buffer (AB) was freshly prepared and consisted of 20 mM HEPES (prepared by diluting 1 M HEPES, pH 7.2), 5 mM $MgCl_2$, 0.01% (v/v) Tween-20 and 1 mM DTT. Stocks of inhibitors (in DMSO) were diluted in AB to obtain 4x working solutions (4% DMSO) and 5 µL was added to the assay plate. BUB1/BUB3 (3.26 µM (486 µg/mL) in storage buffer) was diluted in AB to obtain 13.0 nM of which 5 µL was added to all wells of the assay plate. The assay plate was centrifuged (1 min, 200 *g*) and incubated at RT for 30 min. ATP (4 mM in MilliQ) was diluted in AB to obtain 60 µM of which 5 µL was added to each well. BUB1/BUB3 substrate (1 mM) was diluted in 20 mM HEPES (prepared by diluting 1 M HEPES (pH 7.2) in MilliQ) to obtain 80 µM (this solution was freshly prepared every assay) and further diluted in AB to obtain 300 nM after which 5 µL was added to each well of the assay plate except for background control wells. The assay plate was centrifuged (1 min, 200 *g*) and incubated at RT in the dark for 180 min. IMAP progressive binding buffer A (5x) and IMAP progressive binding buffer B (5x) were mixed in a ratio to obtain 30% buffer A and 70% buffer B, which was subsequently diluted 5x in MilliQ. IMAP progressive binding reagent was diluted 600x in aforementioned mixture of buffer A and B (to obtain a 2x working solution) of which 20 µL was added to each well of the assay plate. The assay plate was centrifuged (1 min, 200 *g*) and incubated at RT in the dark for 90 min. Fluorescence polarization was measured on a CLARIOstar plate reader using the following settings: (i) optic settings → excitation = F: 482-16, dichroic = F: LP 504, emission = F: 530-40, (ii) optic = top optic, (iii) speed/precision = maximum precision, (iv) focus adjustment was performed for every assay and (v) gain adjustment was done by setting the target mP value to 35 mP for one of the MIN control wells. Data was normalized between MIN and MAX controls and data was plotted using GraphPad Prism 8.0 using "Nonlinear regression (curve fit)" and "log(inhibitor) vs. normalized response – Variable slope" to determine pIC_{50} values. For determining the apparent K_M for ATP, the assay was performed as described above, but with variable ATP concentrations (20 nM – 100 µM final concentrations). K_M determination was performed in triplicate and the apparent K_M for ATP was determined to be 8.13 µM. This value was used in the Cheng-Prusoff equation to calculate K_i values.

Experimental – Chemistry

General synthetic procedures

All reagents were purchased from chemical suppliers (Fluorochem, Sigma-Aldrich, Merck, Fisher Scientific) and used without further purification. Solvents (Honeywell, VWR, Biosolve) indicated with "dry" were stored on activated 4 Å molecular sieves (8 to 12 mesh, Acros Organics). Solvents indicated by "degassed" were sonicated while bubbling N_2 through the solvent for 20 min. All reactions were performed at room temperature (RT) under a nitrogen atmosphere, unless stated otherwise. Reactions were monitored by thin layer chromatography (TLC, silica gel 60, UV_{254}, Macherey-Nagel, ref: 818333) and compounds were visualized by UV absorption (254 nm and/or 366 nm) or spray reagent (permanganate (5 g/L $KMnO_4$, 25 g/L K_2CO_3)) followed by heating. Alternatively, reactions were monitored by liquid chromatography-mass spectrometry (LCMS), either on a Thermo Finnigan (Thermo Finnigan LCQ Advantage MAX ion-trap mass spectrometer (ESI+) coupled to a Surveyor HPLC system (Thermo Finnigan) equipped with a Nucleodur C18 Gravity column (50x4.6 mm, 3 µm particle size, Macherey-Nagel)) or a Thermo Fleet (Thermo LCQ Fleet ion-trap mass spectrometer (ESI+) coupled to a Vanquish UHPLC system). LCMS eluent consisted of MeCN in 0.1% TFA (aq.) and LCMS methods were as follows: 0.5 min cleaning with starting gradient, 8 min using specified gradient (linear), 2 min cleaning with 90% MeCN in 0.1% TFA (aq.). LCMS data is reported as follows: instrument (Finnigan or Fleet), gradient (% MeCN in 0.1% TFA (aq.)), retention time (t_r) and mass (as m/z: $[M+H]^+$). Purity of final compounds was determined to be ≥ 95% by integrating UV intensity of spectra generated by either of the LCMS instruments. ^1H and ^{13}C NMR spectra were recorded on a Bruker AV400 (400 and 101 MHz, respectively), Bruker AV500 (500 and 126 MHz, respectively) or Bruker AV600 (600 and 150 MHz, respectively) NMR spectrometer. NMR samples were prepared in deuterated chloroform, methanol or DMSO. Chemical shifts are given in ppm (δ) relative to residual protonated solvent signals ($CDCl_3$ → δ 7.260 (^1H), δ 77.160 (^{13}C), MeOD → δ 3.310 (^1H), δ 49.000 (^{13}C), DMSO → δ 2.500 (^1H), δ 39.520 (^{13}C)). Data was processed by using MestReNova (v. 14) and is reported as follows: chemical shift (δ), multiplicity, coupling constant (*J* in Hz) and integration. Multiplicities are abbreviated as follows: s = singlet, br s = broad singlet, d = doublet, dd = doublet of doublets, ddd = doublet of doublet of

doublets, dt = doublet of triplets, t = triplet, q = quartet, p = pentet, m = multiplet. Purification was done either by manual silica gel column chromatography (using 40-63 µm, 60 Å silica gel, Macherey-Nagel) or automated column chromatography on a Biotage Isolera machine (using pre-packed cartridges with 40-63 µm, 60 Å silica gel (4, 12, 25 or 40 g), Screening Devices). High resolution mass spectrometry (HRMS) spectra were recorded through direct injection of a 1 µM sample either on a Thermo Scientific Q Exactive Orbitrap equipped with an electrospray ion source in positive mode coupled to an Ultimate 3000 system (source voltage = 3.5 kV, capillary temperature = 275°C, resolution R = 240,000 at m/z 400, external lock, mass range m/z = 150-2000) or on a Synapt G2-Si high definition mass spectrometer (Waters) equipped with an electrospray ion source in positive mode (ESI-TOF) coupled to a NanoEquity system with Leu-enkephalin (m/z = 556.2771) as internal lock mass. The eluent for HRMS measurements consisted of a 1:1 (v/v) mixture of MeCN in 0.1% formic acid (aq.) using a flow of 25 mL/min. Compound names were generated by ChemDraw (v. 19.1.21).

1-Cyclopropyl-3-(3-(5-(morpholinomethyl)-1*H*-benzo[*d*]imidazol-2-yl)-1*H*-pyrazol-4-yl)urea (1)

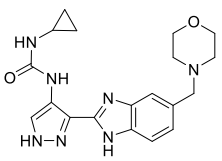

30 (42.1 mg, 141 µmol) and CDI (45.8 mg, 282 µmol) were mixed in dry THF (1.1 mL) and stirred at 66°C for 2.5 h. The obtained solids were collected by filtration, washed with THF (0.5 mL) and dried under reduced pressure. The solids were transferred to a microwave vial, suspended in DMF (0.3 mL) and cyclopropylamine (40 µL, 577 µmol) was added. The vial was sealed and the mixture was stirred at 100°C for 1.5 h. The crude was concentrated at 60°C and purified by automated column chromatography (4 – 15% MeOH/DCM) to afford the product (17.5 mg, 141 µmol, 33%). ^{1}H NMR (500 MHz, MeOD) δ 8.07 (s, 1H), 7.69 – 7.39 (m, 2H), 7.21 (d, *J* = 8.1 Hz, 1H), 3.70 – 3.65 (m, 4H), 3.60 (s, 2H), 2.72 – 2.65 (m, 1H), 2.53 – 2.40 (m, 4H), 1.04 – 0.84 (m, 2H), 0.72 – 0.57 (m, 2H). ^{13}C NMR (126 MHz, MeOD) δ 158.77, 149.31, 144.81, 144.20, 134.95, 134.38, 133.02, 132.04, 131.87, 126.01, 125.07, 123.69, 120.56, 120.00, 119.04, 113.32, 111.86, 67.66, 64.71, 54.59, 23.47, 7.80. LCMS (Finnigan, 0 → 50%): t_r = 5.21 min, m/z: 382.1. HRMS [$C_{19}H_{23}N_7O_2$ + H]$^+$: 382.19860 calculated, 382.1993 found.

4-Methyl-5-(2-((4-morpholinophenyl)amino)pyrimidin-4-yl)thiazol-2-amine (2)

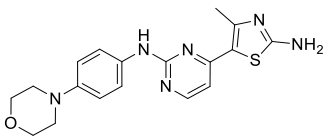

35 (145 mg, 545 µmol) was mixed with **33** (150 mg, 681 µmol) and Na_2CO_3 (57.7 mg, 545 µmol) in 2-methoxyethanol (0.3 mL) and stirred at 124°C for 16 h. The mixture was concentrated at 70°C, brought onto Celite and purified by silica gel chromatography (2 – 5% MeOH/DCM). The impure product was subsequently suspended in MeOH (3 mL), sonicated, filtered and the solids were washed with MeOH (3 mL). The solids were collected and dried to afford the product (91.0 mg, 248 µmol, 46%). ^{1}H NMR (500 MHz, DMSO) δ 9.19 (s, 1H), 8.27 (d, *J* = 5.4 Hz, 1H), 7.65 – 7.58 (m, 2H), 7.47 (s, 2H), 6.91 – 6.83 (m, 2H), 6.80 (d, *J* = 5.5 Hz, 1H), 3.76 – 3.70 (m, 4H), 3.05 – 3.00 (m, 4H), 2.42 (s, 3H). ^{13}C NMR (126 MHz, DMSO) δ 168.72, 159.59, 158.62, 157.56, 151.70, 145.93, 133.13, 120.02, 118.22, 115.55, 106.26, 66.20, 49.34, 18.43. LCMS (Finnigan, 0 → 50%): t_r = 5.79 min, m/z: 369.3. HRMS [$C_{18}H_{20}N_6OS$ + H]$^+$: 369.14921 calculated, 369.14794 found.

2-((4-((3-Ethynylphenyl)amino)-7-(2-methoxyethoxy)quinazolin-6-yl)oxy)ethan-1-ol (3)

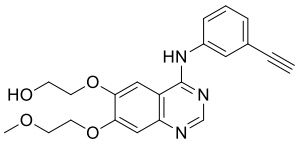

44 (41 mg, 98 µmol) was dissolved in 0.4 M NaOH in MeOH (370 µL) and stirred for 2 h. The mixture was diluted in a mixture of H_2O (30 mL) and brine (2 mL) and the product extracted with $CHCl_3$ (30 mL). The organic layer was concentrated as such and purified by automated column chromatography (4 – 20% MeOH/DCM) to afford the product (10 mg, 27 µmol, 27%). ^{1}H NMR (600 MHz, MeOD) δ 8.41 (s, 1H), 7.91 (t, *J* = 1.9 Hz, 1H), 7.76 (ddd, *J* = 8.2, 2.3, 1.1 Hz, 1H), 7.73 – 7.69 (m, 1H), 7.36 (t, *J* = 7.9 Hz, 1H), 7.25 (dt, *J* = 7.7, 1.2 Hz, 1H), 7.15 – 7.13 (m, 1H), 4.30 – 4.27 (m, 2H), 4.27 – 4.24 (m, 2H), 4.01 – 3.96 (m, 2H), 3.86 – 3.83 (m, 2H), 3.51 (s, 1H), 3.46 (s, 3H). ^{13}C NMR (151 MHz, MeOD) δ 158.44, 155.95, 153.93, 150.54, 147.58, 140.62, 129.89, 128.72, 127.05, 124.29, 124.15, 110.68, 108.31, 103.98, 84.32, 78.71, 72.14,

71.68, 69.49, 61.54, 59.37. LCMS (Finnigan, 10 → 90%): t_r = 5.02 min, m/z: 380.2. HRMS [$C_{21}H_{21}N_3O_4$ + H]$^+$: 380.16048 calculated, 380,1615 found.

1-Cyclopentyl-3-(1*H*-pyrrolo[2,3-*b*]pyridin-5-yl)-1*H*-pyrazolo[3,4-*d*]pyrimidin-4-amine (4)

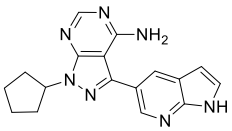

46 (20 mg, 61 µmol), 7-azaindole-5-boronic acid pinacol ester (17.8 mg, 72.9 µmol) and Na_2CO_3 (12.9 mg, 122 µmol) were mixed in degassed DMF (0.5 mL) and H_2O (50 µL). $Pd(PPh_3)_4$ (4.9 mg, 4.3 µmol) was added and the mixture was stirred at 100°C for 17 h. The mixture was poured into H_2O (20 mL) and the product extracted with EtOAc (3x20 mL). The combined organic layers were washed with brine (60 mL), dried over Na_2SO_4, filtered and concentrated. The crude was purified by automated column chromatography (0 – 40% MeOH/DCM) to afford the product (13.5 mg, 42.3 µmol, 70%). ^{1}H NMR (500 MHz, MeOD) δ 8.50 (d, *J* = 2.0 Hz, 1H), 8.25 (d, *J* = 2.0 Hz, 1H), 8.24 (s, 1H), 7.46 (d, *J* = 3.5 Hz, 1H), 6.59 (d, *J* = 3.5 Hz, 1H), 5.27 (p, *J* = 7.6 Hz, 1H), 2.21 – 2.13 (m, 4H), 2.04 – 1.94 (m, 2H), 1.79 – 1.69 (m, 2H). ^{13}C NMR (126 MHz, MeOD) δ 159.47, 156.07, 154.48, 149.11, 143.89, 143.02, 129.89, 128.13, 122.13, 121.78, 101.76, 99.57, 58.73, 32.94, 25.38. LCMS (Finnigan, 0 → 50%): t_r = 7.34 min, m/z: 320.2. HRMS [$C_{17}H_{17}N_7$ + H]$^+$: 320.16182 calculated, 320.1627 found.

(3,4-Dinitrophenyl)(morpholino)methanone (26)

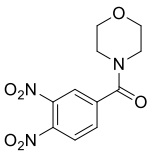

3,4-Dinitrobenzoic acid (15.0 g, 70.7 mmol) was dissolved in dry THF (150 mL) after which dry DMF (0.15 mL) and $SOCl_2$ (7.2 mL, 99 mmol) were added. The mixture was heated to 70°C and stirred for 2.5 h after which the mixture was cooled down to 0°C. Et_3N (14.9 mL, 107 mmol) was added dropwise over 15 min and subsequently morpholine (10.7 mL, 124 mmol) was added dropwise over 10 min. The mixture was allowed to warm up to RT and stirred overnight. H_2O (375 mL) was added and stirring was continued vigorously for 1 h after which the mixture was cooled down to 0°C and filtered. The solids were washed with ice cold H_2O (100 mL), collected and traces of water were removed by coevaporation with MeOH several times to afford the product (18.4 g, 65.4 mmol, 93%). ^{1}H NMR (400 MHz, DMSO) δ 8.31 (d, *J* = 1.7 Hz, 1H), 8.30 (d, *J* = 8.2 Hz, 1H), 8.01 (dd, *J* = 8.3, 1.7 Hz, 1H), 3.71 – 3.60 (m, 4H), 3.59 – 3.49 (m, 2H), 3.37 – 3.27 (m, 2H). ^{13}C NMR (101 MHz, DMSO) δ 165.09, 142.04, 141.35, 132.85, 126.22, 124.30, 65.91, 65.75, 47.41, 42.10.

4-(3,4-Dinitrobenzyl)morpholine (27)

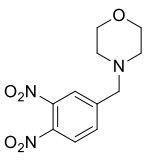

$NaBH_4$ (5.25 g, 139 mmol) was suspended in dry THF (193 mL) and cooled down to 0°C after which boron trifluoride etherate (17.1 mL, 139 mmol) was added. Subsequently, solid **26** (18.4 g, 65.4 mmol) was added after which the mixture was allowed to warm to RT and stirred for 3.5 h. The mixture was cooled down to 0°C and MeOH (160 mL) was added dropwise over 20 min (H_2 evolution). The resulting suspension was allowed to warm to RT, further heated to 70°C and stirred for 75 min (H_2 evolution). The mixture was concentrated, redissolved in EtOAc (200 mL) and poured into half sat. $NaHCO_3$ (200 mL). The organic layer was isolated and the water layer extracted with EtOAc (200 mL). The combined organic layers were washed with H_2O (200 mL), the organic layer was separated and the water layer extracted with EtOAc (100 mL). The combined organic layers were washed with brine (300 mL), dried over Na_2SO_4, filtered and concentrated. The obtained powder was grounded, suspended in MeOH (55 mL) and warmed up until fully dissolved. The solution was slowly cooled down to RT, further cooled on ice and kept on ice for 25 min. The mixture was filtered and the solids were washed with ice cold MeOH (40 mL) to afford the product (13.5 g, 50.4 mmol, 77%). ^{1}H NMR (400 MHz, $CDCl_3$) δ 7.87 (d, *J* = 1.6 Hz, 1H), 7.84 (d, *J* = 8.3 Hz, 1H), 7.71 (dd, *J* = 8.3, 1.6 Hz, 1H), 3.66 – 3.61 (m, 4H), 3.59 (s, 2H), 2.45 – 2.39 (m, 4H). ^{13}C NMR (101 MHz, $CDCl_3$) δ 146.54, 143.01, 141.09, 132.98, 125.06, 124.66, 66.65, 61.35, 53.36. LCMS (Finnigan, 10 → 90%): t_r = 4.03 min, m/z: 268.1.

4-(Morpholinomethyl)benzene-1,2-diamine (28)

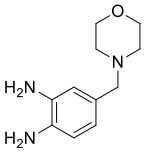

27 (2.50 g, 9.35 mmol) was suspended in absolute EtOH (75 mL) and this mixture was subsequently degassed by bubbling N_2 through the mixture while sonicating for 20 min. 10% Pd/C (250 mg) was added and the atmosphere was exchanged for H_2. The reaction was vigorously stirred for 2 h while bubbling H_2 through the mixture. The atmosphere was exchanged for N_2, the mixture was filtered over Celite and subsequently concentrated to afford the product (1.58 g, 9.35 mmol, 81%). ^{1}H NMR (400 MHz, MeOD) δ 6.63 (d, *J* = 1.8 Hz, 1H), 6.60 (d, *J* = 7.8 Hz, 1H), 6.51 (dd, *J* = 7.9, 1.8 Hz, 1H), 3.63 – 3.58 (m, 4H), 3.27 (s, 2H), 2.41 – 2.31 (m, 4H). ^{13}C NMR (101 MHz, MeOD) δ 135.81, 135.32, 128.48, 122.11, 119.00, 117.20, 67.51, 64.25, 54.39. LCMS (Fleet, 0 → 50%): t_r = 0.86 min, m/z: 208.1.

4-((2-(4-Nitro-1*H*-pyrazol-3-yl)-1*H*-benzo[*d*]imidazol-5-yl)methyl)morpholine (29)

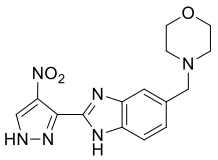

28 (3.55 g, 17.1 mmol), 4-nitro-1*H*-pyrazole-3-carboxylic acid (2.53 g, 16.1 mmol), EDC·HCl (3.38 g, 17.7 mmol) and HOBt (2.32 g, 17.1 mmol) were mixed in dry DMF (39 mL) and stirred for 20 h. The mixture was concentrated at 60°C after which AcOH (49 mL) was added. The mixture was heated to 118°C and stirred for 2.5 h. The mixture was concentrated at 80°C and traces of AcOH were removed by coevaporated with toluene (4x20 mL). The crude was brought onto Celite and purified by silica gel chromatography (5 – 9% MeOH/DCM) to afford the product (3.07 g, 9.35 mmol, 55%). ^{1}H NMR (400 MHz, MeOD) δ 8.60 (s, 1H), 7.68 (s, 1H), 7.60 (d, *J* = 8.3 Hz, 1H), 7.28 (d, *J* = 8.4 Hz, 1H), 3.98 (s, 2H), 3.78 – 3.66 (m, 4H), 2.89 – 2.78 (m, 4H). ^{13}C NMR (101 MHz, MeOD) δ 144.63, 139.63, 139.44, 136.69, 134.62, 133.79, 128.93, 126.95, 118.88, 116.50, 66.10, 63.04, 53.34. LCMS (Finnigan, 0 → 50%): t_r = 4.60 min, m/z: 329.1.

3-(5-(Morpholinomethyl)-1*H*-benzo[*d*]imidazol-2-yl)-1*H*-pyrazol-4-amine (30)

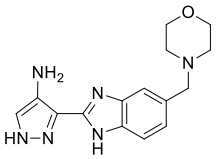

29 (398 mg, 1.21 mmol) was suspended in degassed MeOH (14 mL). 10% Pd/C (56 mg) was added and the atmosphere was exchanged for H_2. The reaction was vigorously stirred for 100 min while bubbling H_2 through the mixture. The atmosphere was exchanged for N_2, the mixture was filtered over Celite and subsequently concentrated. The crude was purified by silica gel chromatography (6 – 9% MeOH (containing 10% sat. NH_4OH (aq.))/DCM) to afford the product (260 mg, 1.21 mmol, 72%). ^{1}H NMR (500 MHz, MeOD) δ 7.53 – 7.40 (m, 2H), 7.31 (s, 1H), 7.10 (dd, *J* = 8.3, 1.3 Hz, 1H), 3.61 – 3.54 (m, 4H), 3.45 (s, 2H), 2.38 – 2.30 (m, 4H). ^{13}C NMR (126 MHz, MeOD) δ 149.40 (br), 139.52 (br), 132.38 (br), 132.14, 130.90, 125.30, 118.67 (br), 116.01 (br), 67.49, 64.48, 54.33. LCMS (Finnigan, 0 → 50%): t_r = 0.92 min, m/z: 299.1.

4-(4-Nitrophenyl)morpholine (31)

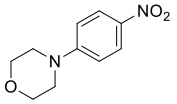

1-Fluoro-4-nitrobenzene (510 mg, 3.61 mmol) was dissolved in MeCN (8 mL) after which morpholine (350 µL, 4.00 mmol) and Et_3N (555 µL, 3.98 mmol) were added. The mixture was heated to 82°C, stirred for 15 h and subsequently poured into H_2O (100 mL). The product was extracted with EtOAc (3x75 mL) after which the combined organic layers were washed with brine (200 mL), dried over Na_2SO_4, filtered and concentrated. The crude was purified by silica gel chromatography (0 – 1% MeOH (containing 10% sat. NH_4OH (aq.))/DCM) to afford the product (701 mg, 3.37 mmol, 93%). ^{1}H NMR (400 MHz, $CDCl_3$) δ 8.10 – 8.04 (m, 2H), 6.82 – 6.75 (m, 2H), 3.87 – 3.79 (m, 4H), 3.38 – 3.31 (m, 4H). ^{13}C NMR (101 MHz, $CDCl_3$) δ 155.00, 138.78, 125.85, 112.55, 66.35, 47.04.

4-Morpholinoaniline (32)

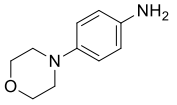

31 (2.51 g, 12.1 mmol) was suspended in MeOH (150 mL) and this mixture was subsequently degassed by bubbling N_2 through the mixture while sonicating for 20 min. 10% Pd/C (251 mg) was added and the atmosphere was exchanged for H_2. The reaction was vigorously stirred for 5 h while bubbling H_2 through the mixture. The atmosphere was exchanged for N_2, the mixture was filtered over Celite and subsequently concentrated. The crude was purified by silica gel chromatography (6 – 20% MeOH (containing 10% sat. NH_4OH

(aq.))/DCM) to afford the product (1.97 g, 11.0 mmol, 91%). ^{1}H NMR (400 MHz, $CDCl_3$) δ 6.81 – 6.76 (m, 2H), 6.66 – 6.61 (m, 2H), 3.87 – 3.80 (m, 4H), 3.46 (s, 2H), 3.05 – 2.97 (m, 4H). ^{13}C NMR (101 MHz, $CDCl_3$) δ 144.21, 140.37, 118.07, 116.07, 66.98, 51.01.

1-(4-Morpholinophenyl)guanidine (33)

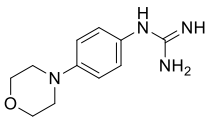

32 (800 mg, 4.49 mmol) was suspended in EtOH (2.65 mL) and cooled down to 0°C. Concentrated HCl (aq.) (300 µL, 3.73 mmol) and cyanamide (50% w/w aq.) (660 µL, 16.6 mmol) were added and the mixture was heated to 78°C and stirred for 4 h. The reaction was allowed to cool down to RT after which concentrated HCl (aq.) (300 µL, 3.73 mmol) was added and the mixture was heated to 78°C and stirred for 4 h. The reaction was cooled to RT and concentrated HCl (466 µL, 5.70 mmol) was added after which the mixture was heated to 78°C and stirred overnight. The crude was carefully poured into a mixture of DCM (100 mL) and 1 M $NaHCO_3$ (100 mL) and stirred. The formed precipitate was collected by filtration of the two layers. The solids were collected, suspended in H_2O (10 mL) and sonicated for a few minutes. The suspension was filtered, washed with acetone (20 mL) after which the solids were collected and concentrated to afford the product (948 mg, 4.31 mmol, 96%). ^{1}H NMR (400 MHz, DMSO) δ 7.29 (br s, 4H), 6.89 (s, 4H), 3.76 – 3.69 (m, 4H), 3.08 – 3.01 (m, 4H). ^{13}C NMR (101 MHz, DMSO) δ 160.18, 155.01 (br), 147.78 (br), 124.73, 116.16, 66.19, 48.99.

1-(2-Amino-4-methylthiazol-5-yl)ethan-1-one hydrochloride (34)

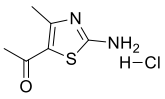

Thiourea (250 mg, 3.28 mmol) was dissolved in MeOH (2.5 mL) and cooled down to 0°C. Pyridine (106 µL, 1.31 mmol) and 3-chloropentane-2,4-dione (372 µL, 3.29 mmol) were added after which the mixture was allowed to warm to RT and stirred for 2 h. The mixture was concentrated, subsequently suspended in EtOAc (3 mL) and filtered. The solids were washed with EtOAc (5 mL), collected and dried to afford the product (562 mg, 2.91 mmol, 89%). ^{1}H NMR (400 MHz, DMSO) δ 7.83 (s, 2H), 2.40 (s, 3H), 2.32 (s, 3H). ^{13}C NMR (101 MHz, DMSO) δ 188.27, 170.51, 157.72, 121.30, 29.49, 18.35.

N'-(5-(3-(Dimethylamino)acryloyl)-4-methylthiazol-2-yl)-*N*,*N*-dimethylformimidamide (35)

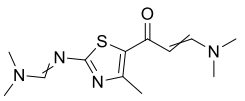

34 (500 mg, 2.60 mmol) was mixed with DMF-DMA (1.5 mL, 11 mmol) and stirred at 105°C for 18 h. The mixture was concentrated and subsequently purified by silica gel chromatography (1 – 6% MeOH/DCM) to afford the product (484 mg, 1.82 mmol, 70%). ^{1}H NMR (400 MHz, $CDCl_3$) δ 8.16 (s, 1H), 7.61 (d, *J* = 12.2 Hz, 1H), 5.28 (d, *J* = 12.2 Hz, 1H), 3.05 (s, 3H), 3.03 (br s, 3H), 3.02 (s, 3H), 2.81 (br s, 3H), 2.57 (s, 3H). ^{13}C NMR (101 MHz, $CDCl_3$) δ 181.50, 173.60, 155.89, 153.98, 152.89, 126.60, 95.03, 40.90, 35.00, 18.28. LCMS (Finnigan, 0 → 50%): t_r = 5.33 min, m/z: 267.1.

Ethyl 4-(benzyloxy)-3-hydroxybenzoate (36)

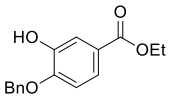

Ph_3P (6.00 g, 23.1 mmol) and DIAD (4.8 mL, 23 mmol) were dissolved in dry THF (147 mL) and cooled down to 0°C. Benzyl alcohol (2.3 mL, 22 mmol) was added and the mixture was stirred for 5 min. A solution of ethyl 3,4-dihydroxybenzoate (4.00 g, 22.0 mmol) in THF (37 mL) was added and the mixture was stirred for 30 min after which the reaction was allowed to warm to RT and continued to stir for 70 h. The mixture was concentrated, loaded onto Celite and purified by automated column chromatography (twice, 5 – 40% Et_2O/pentane) to afford the product (2.43 g, 8.93 mmol, 41%). ^{1}H NMR (400 MHz, $CDCl_3$) δ 7.63 (d, *J* = 2.1 Hz, 1H), 7.60 (dd, *J* = 8.4, 2.1 Hz, 1H), 7.47 – 7.33 (m, 5H), 6.94 (d, *J* = 8.5 Hz, 1H), 5.78 (s, 1H), 5.16 (s, 2H), 4.33 (q, *J* = 7.1 Hz, 2H), 1.37 (t, *J* = 7.1 Hz, 3H). ^{13}C NMR (101 MHz, $CDCl_3$) δ 166.41, 149.59, 145.51, 135.70, 128.75, 128.24, 127.98, 124.10, 122.74, 115.93, 111.29, 71.19, 60.91, 14.45. Regioselectivity was confirmed by ^{1}H-^{1}H-ROESY NMR analysis. LCMS (Finnigan, 10 → 90%): t_r = 7.66 min, m/z: not observed.

Ethyl 3-(2-acetoxyethoxy)-4-(benzyloxy)benzoate (37)

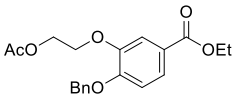

36 (2.40 g, 8.81 mmol) was dissolved in dry DMF (8.8 mL). K_2CO_3 (2.44 g, 17.6 mmol) and 2-bromoethyl acetate (1.5 mL, 13 mmol) were added and the mixture was stirred at 100°C for 3 h. The mixture was poured into H_2O (200 mL) and the product extracted with DCM (3x150 mL). The combined organic layers were washed with brine (200 mL), dried over Na_2SO_4, filtered and concentrated. The crude was purified by silica gel chromatography (10 – 20% Et_2O/pentane) to afford the product (2.26 g, 6.30 mmol, 72%). ^{1}H NMR (400 MHz, $CDCl_3$) δ 7.66 (dd, *J* = 8.4, 2.0 Hz, 1H), 7.61 (d, *J* = 2.0 Hz, 1H), 7.46 – 7.41 (m, 2H), 7.41 – 7.35 (m, 2H), 7.34 – 7.29 (m, 1H), 6.93 (d, *J* = 8.5 Hz, 1H), 5.19 (s, 2H), 4.49 – 4.41 (m, 2H), 4.34 (q, *J* = 7.1 Hz, 2H), 4.31 – 4.27 (m, 2H), 2.07 (s, 3H), 1.37 (t, *J* = 7.1 Hz, 3H). ^{13}C NMR (101 MHz, $CDCl_3$) δ 171.14, 166.32, 152.90, 148.18, 136.57, 128.73, 128.17, 127.25, 124.47, 123.59, 115.71, 113.41, 70.92, 67.65, 62.97, 60.99, 21.00, 14.52. LCMS (Finnigan, 10 → 90%): t_r = 8.27 min, m/z: not observed.

Ethyl 3-(2-acetoxyethoxy)-4-hydroxybenzoate (38)

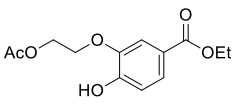

37 (2.26 g, 6.30 mmol) was dissolved in degassed MeOH (63 mL). 10% Pd/C (226 mg) was added and the atmosphere was exchanged for H_2. The reaction was vigorously stirred for 2.5 h while bubbling H_2 through the mixture. The atmosphere was exchanged for N_2, the mixture was filtered over Celite and subsequently concentrated to afford the product (1.65 g, 6.14 mmol, 98%). ^{1}H NMR (400 MHz, $CDCl_3$) δ 7.66 (dd, *J* = 8.3, 1.9 Hz, 1H), 7.55 (d, *J* = 1.9 Hz, 1H), 6.95 (d, *J* = 8.4 Hz, 1H), 6.32 (s, 1H), 4.50 – 4.43 (m, 2H), 4.33 (q, *J* = 7.2 Hz, 2H), 4.31 – 4.27 (m, 2H), 2.10 (s, 3H), 1.37 (t, *J* = 7.1 Hz, 3H). ^{13}C NMR (101 MHz, $CDCl_3$) δ 171.29, 166.38, 150.50, 145.23, 124.95, 122.68, 114.64, 113.60, 67.92, 62.63, 60.97, 21.00, 14.50. LCMS (Finnigan, 10 → 90%): t_r = 6.23 min, m/z: not observed.

Ethyl 3-(2-acetoxyethoxy)-4-(2-methoxyethoxy)benzoate (39)

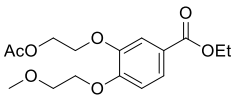

38 (1.62 g, 6.03 mmol) was dissolved in dry DMF (6 mL). K_2CO_3 (1.67 g, 12.1 mmol) and 1-bromo-2-methoxyethane (850 µL, 9.04 mmol) were added and the mixture was stirred at 100°C for 2 h. The mixture was poured into H_2O (200 mL) and the product extracted with DCM (3x150 mL). The combined organic layers were washed with brine (200 mL), dried over Na_2SO_4, filtered and concentrated. The crude was purified by silica gel chromatography (25 – 50% EtOAc/pentane) to afford the product (1.89 g, 5.80 mmol, 96%). ^{1}H NMR (400 MHz, $CDCl_3$) δ 7.68 (dd, *J* = 8.4, 2.0 Hz, 1H), 7.58 (d, *J* = 2.0 Hz, 1H), 6.91 (d, *J* = 8.5 Hz, 1H), 4.48 – 4.41 (m, 2H), 4.34 (q, *J* = 7.1 Hz, 2H), 4.28 – 4.23 (m, 2H), 4.22 – 4.17 (m, 2H), 3.82 – 3.75 (m, 2H), 3.45 (s, 3H), 2.09 (s, 3H), 1.37 (t, *J* = 7.1 Hz, 3H). ^{13}C NMR (101 MHz, $CDCl_3$) δ 171.06, 166.27, 153.06, 148.00, 124.44, 123.49, 115.62, 112.85, 70.87, 68.64, 67.53, 62.95, 60.90, 59.39, 20.95, 14.46.

Ethyl 5-(2-acetoxyethoxy)-4-(2-methoxyethoxy)-2-nitrobenzoate (40)

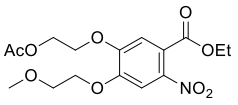

39 (1.86 g, 5.71 mmol) was dissolved in Ac_2O (15 mL) and cooled down to 0°C. $Cu(NO_3)_2{\cdot}3H_2O$ (3.45 g, 14.3 mmol) was added and the mixture was stirred at 0°C for 1 h. The mixture was allowed to warm to RT and stirred until the mild exothermic reaction had occurred. The reaction was cooled down to 0°C, diluted with H_2O (200 mL) and the product extracted with DCM (3x150 mL). The combined organic layers were washed with 1 M $NaHCO_3$ (aq.) (200 mL), brine (200 mL) and subsequently dried over Na_2SO_4, filtered and concentrated. The crude was purified by silica gel chromatography (30 – 60% Et_2O/pentane) to afford the product (1.55 g, 4.17 mmol, 73%). ^{1}H NMR (400 MHz, $CDCl_3$) δ 7.49 (s, 1H), 7.11 (s, 1H), 4.50 – 4.43 (m, 2H), 4.36 (q, *J* = 7.2 Hz, 2H), 4.34 – 4.27 (m, 2H), 4.26 – 4.20 (m, 2H), 3.83 – 3.76 (m, 2H), 3.45 (s, 3H), 2.09 (s, 3H), 1.34 (t, *J* = 7.2 Hz, 3H). ^{13}C NMR (101 MHz, $CDCl_3$) δ 170.94, 165.72, 151.90, 150.26, 141.74, 122.09, 113.21, 109.31, 70.68, 69.45, 67.67, 62.58, 62.40, 59.47, 20.92, 13.90.

Ethyl 5-(2-acetoxyethoxy)-2-amino-4-(2-methoxyethoxy)benzoate (41)

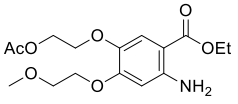

40 (657 mg, 1.77 mmol) was dissolved in degassed MeOH (5 mL). 5% Pt/C (66 mg) was added and the atmosphere was exchanged for H_2. The reaction was vigorously stirred for 1 h while bubbling H_2 through the mixture. The atmosphere was exchanged for N_2, the mixture was filtered over Celite and

subsequently concentrated. The crude was brought onto Celite and purified by automated column chromatography (50 – 100% Et_2O/pentane) to afford the product (396 mg, 1.16 mmol, 66%). ^{1}H NMR (400 MHz, $CDCl_3$) δ 7.41 (s, 1H), 6.13 (s, 1H), 4.38 – 4.34 (m, 2H), 4.27 (q, *J* = 7.1 Hz, 2H), 4.13 – 4.07 (m, 4H), 3.77 – 3.73 (m, 2H), 3.42 (s, 3H), 2.08 (s, 3H), 1.35 (t, *J* = 7.1 Hz, 3H) (the –NH_2 was not observed). ^{13}C NMR (101 MHz, $CDCl_3$) δ 171.17, 167.68, 155.38, 148.04, 139.31, 118.98, 103.06, 100.76, 70.74, 69.16, 68.06, 63.39, 60.20, 59.32, 21.00, 14.52.

2-((7-(2-Methoxyethoxy)-4-oxo-3,4-dihydroquinazolin-6-yl)oxy)ethyl acetate (42)

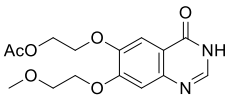

41 (629 mg, 1.84 mmol) and NH_4HCO_2 (117 mg, 1.85 mmol) were mixed in formamide (1.9 mL) and stirred at 160°C for 3.5 h. The mixture was poured into H_2O (25 mL) and the product extracted with DCM (3x25 mL). The combined organic layers were washed with brine (25 mL), dried over Na_2SO_4, filtered and concentrated. The crude was purified by automated column chromatography (1 – 10% MeOH/DCM) to afford the product (357 mg, 1.11 mmol, 60%). ^{1}H NMR (400 MHz, $CDCl_3$) δ 7.99 (s, 1H), 7.51 (s, 1H), 7.07 (s, 1H), 4.47 – 4.42 (m, 2H), 4.30 – 4.25 (m, 2H), 4.25 – 4.19 (m, 2H), 3.82 – 3.75 (m, 2H), 3.41 (s, 3H), 2.05 (s, 3H) (the –NH was not observed). ^{13}C NMR (101 MHz, $CDCl_3$) δ 171.08, 162.23, 154.88, 148.35, 145.45, 142.95, 115.67, 109.15, 107.06, 70.48, 68.60, 67.08, 62.51, 59.31, 20.84. LCMS (Finnigan, 10 → 90%): t_r = 3.86 min, m/z: 323.1.

2-((4-Chloro-7-(2-methoxyethoxy)quinazolin-6-yl)oxy)ethyl acetate (43)

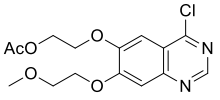

42 (332 mg, 1.03 mmol) was dissolved in $POCl_3$ (2 mL) and the mixture was stirred at 105°C for 1.5 h. The mixture was poured into H_2O (50 mL) and the product extracted with DCM (3x50 mL). The combined organic layers were washed with brine (50 mL), dried over Na_2SO_4, filtered and concentrated. The crude was purified by automated column chromatography (1 – 10% MeOH/DCM) to afford the product (280 mg, 820 µmol, 80%). ^{1}H NMR (400 MHz, $CDCl_3$) δ 8.86 (s, 1H), 7.42 (s, 1H), 7.34 (s, 1H), 4.57 – 4.53 (m, 2H), 4.41 – 4.37 (m, 2H), 4.35 – 4.30 (m, 2H), 3.91 – 3.85 (m, 2H), 3.49 (s, 3H), 2.12 (s, 3H). ^{13}C NMR (101 MHz, $CDCl_3$) δ 171.04, 159.30, 156.45, 152.74, 150.71, 149.19, 119.55, 107.99, 104.48, 70.46, 69.09, 67.34, 62.41, 59.59, 21.00. LCMS (Finnigan, 10 → 90%): t_r = 5.62 min, m/z: 341.0.

2-((4-((3-Ethynylphenyl)amino)-7-(2-methoxyethoxy)quinazolin-6-yl)oxy)ethyl acetate (44)

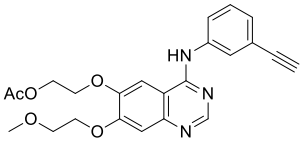

43 (30 mg, 87 µmol) was dissolved in 2-propanol (0.6 mL). 3-Ethynylaniline (10 µL, 96 µmol) was added and the mixture was stirred at 82°C for 1.5 h. The mixture was concentrated and purified by automated column chromatography (1 – 10% MeOH/DCM) to afford the product (36 mg, 87 µmol, quant.). ^{1}H NMR (400 MHz, MeOD) δ 8.44 (s, 1H), 7.90 (d, *J* = 1.9 Hz, 1H), 7.80 (s, 1H), 7.75 (d, *J* = 8.1 Hz, 1H), 7.36 (t, *J* = 7.9 Hz, 1H), 7.26 (d, *J* = 7.6 Hz, 1H), 7.18 (s, 1H), 4.54 – 4.49 (m, 2H), 4.40 (t, *J* = 4.6 Hz, 2H), 4.32 – 4.27 (m, 2H), 3.88 – 3.82 (m, 2H), 3.47 (d, *J* = 1.9 Hz, 4H), 2.09 (s, 3H). LCMS (Finnigan, 0 → 50%): t_r = 8.25 min, m/z: 422.2.

3-Iodo-1*H*-pyrazolo[3,4-*d*]pyrimidin-4-amine (45)

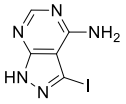

1*H*-Pyrazolo[3,4-*d*]pyrimidin-4-amine (157 mg, 1.16 mmol) and *N*-iodosuccinimide (287 mg, 1.28 mmol) were suspended in dry DMF (0.65 mL), heated to 85°C and stirred for 18 h. The mixture was filtered and the solids washed with ice cold EtOH (2 mL). The solids were collected and concentrated to afford the product (191 mg, 0.733 mmol, 63%).^{1}H NMR (400 MHz, DMSO) δ 8.17 (s, 1H), 7.62 (br s, 1H), 6.69 (br s, 1H) (the –NH was not observed).

1-Cyclopentyl-3-iodo-1*H*-pyrazolo[3,4-*d*]pyrimidin-4-amine (46)

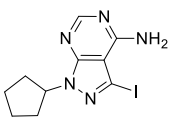

45 (100 mg, 0.383 mmol) and K_2CO_3 (212 mg, 1.53 mmol) were suspended in dry DMF (2.5 mL) after which bromocyclopentane (45 µL, 0.42 mmol) was added and the mixture was stirred at 80°C for 4 h. The mixture was filtered and the solids dissolved in a mixture of H_2O (40 mL) and EtOAc (40 mL). The organic layer was separated and the water layer extracted with EtOAc (40 mL). The combined organic layers were

washed with brine (80 mL), dried over Na_2SO_4, filtered and concentrated. The crude was purified by automated column chromatography (0 – 100% MeOH/DCM) to afford the product (74.7 mg, 0.227 mmol, 59%). ^{1}H NMR (400 MHz, MeOD) δ 8.18 (s, 1H), 5.13 (p, *J* = 7.6 Hz, 1H), 2.16 – 1.99 (m, 4H), 1.99 – 1.85 (m, 2H), 1.79 – 1.60 (m, 2H). ^{13}C NMR (101 MHz, MeOD) δ 158.20, 155.70, 153.39, 104.41, 86.64, 58.78, 32.63, 24.84. LCMS (Finnigan, 0 → 50%): t_r = 7.48 min, m/z: 330.0.

Supplementary information

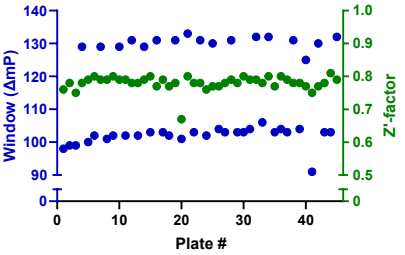

Supplementary Figure 1 | Quality parameters during primary screen. In blue, the assay window (ΔmP) per plate. In green, the Z'-factor per plate.

References

1. Sung, H., Ferlay, J., Siegel, R. L., Laversanne, M., Soerjomataram, I., Jemal, A. & Bray, F. Global Cancer Statistics 2020: GLOBOCAN Estimates of Incidence and Mortality Worldwide for 36 Cancers in 185 Countries. *CA. Cancer J. Clin.* **71**, 209–249 (2021).
2. Duffy, M. J., Harbeck, N., Nap, M., Molina, R., Nicolini, A., Senkus, E. & Cardoso, F. Clinical use of biomarkers in breast cancer: Updated guidelines from the European Group on Tumor Markers (EGTM). *Eur. J. Cancer* **75**, 284–298 (2017).
3. Waks, A. G. & Winer, E. P. Breast Cancer Treatment: A Review. *JAMA* **321**, 288 (2019).
4. Howlader, N., Altekruse, S. F., Li, C. I., Chen, V. W., Clarke, C. A., Ries, L. A. G. & Cronin, K. A. US Incidence of Breast Cancer Subtypes Defined by Joint Hormone Receptor and HER2 Status. *JNCI J. Natl. Cancer Inst.* **106**, (2014).
5. Jordan, V. C. Selective Estrogen Receptor Modulation: A Personal Perspective. *Cancer Res.* **61**, 5683–5687 (2001).
6. Johnston, S. R. D. & Dowsett, M. Aromatase inhibitors for breast cancer: lessons from the laboratory. *Nat. Rev. Cancer* **3**, 821–831 (2003).
7. Harbeck, N., Penault-Llorca, F., Cortes, J., Gnant, M., Houssami, N., Poortmans, P., Ruddy, K., Tsang, J. & Cardoso, F. Breast cancer. *Nat. Rev. Dis. Primer* **5**, 66 (2019).
8. Hudis, C. A. Trastuzumab — Mechanism of Action and Use in Clinical Practice. *N. Engl. J. Med.* **357**, 39–51 (2007).
9. Xuhong, J.-C., Qi, X.-W., Zhang, Y. & Jiang, J. Mechanism, safety and efficacy of three tyrosine kinase inhibitors lapatinib, neratinib and pyrotinib in HER2-positive breast cancer. *Am. J. Cancer Res.* **9**, 2103–2119 (2019).
10. Dominguez-Brauer, C., Thu, K. L., Mason, J. M., Blaser, H., Bray, M. R. & Mak, T. W. Targeting Mitosis in Cancer: Emerging Strategies. *Mol. Cell* **60**, 524–536 (2015).
11. Kops, G. J. P. L., Weaver, B. A. A. & Cleveland, D. W. On the road to cancer: aneuploidy and the mitotic checkpoint. *Nat. Rev. Cancer* **5**, 773–785 (2005).
12. Siemeister, G., Mengel, A., Fernández-Montalván, A. E., Bone, W., Schröder, J., Zitzmann-Kolbe, S., Briem, H., Prechtl, S., Holton, S. J., Mönning, U., von Ahsen, O., Johanssen, S., Cleve, A., Pütter, V., Hitchcock, M., von Nussbaum, F., Brands, M., Ziegelbauer, K. & Mumberg, D. Inhibition of BUB1 Kinase by BAY 1816032 Sensitizes Tumor Cells toward Taxanes, ATR, and PARP Inhibitors *In Vitro* and *In Vivo*. *Clin. Cancer Res.* **25**, 1404–1414 (2019).
13. Musacchio, A. & Salmon, E. D. The spindle-assembly checkpoint in space and time. *Nat. Rev. Mol. Cell Biol.* **8**, 379–393 (2007).
14. Zhang, G., Kruse, T., López-Méndez, B., Sylvestersen, K. B., Garvanska, D. H., Schopper, S., Nielsen, M. L. & Nilsson, J. Bub1 positions Mad1 close to KNL1 MELT repeats to promote checkpoint signalling. *Nat. Commun.* **8**, 15822 (2017).
15. Zhang, G., Lischetti, T., Hayward, D. G. & Nilsson, J. Distinct domains in Bub1 localize RZZ and BubR1 to kinetochores to regulate the checkpoint. *Nat. Commun.* **6**, 7162 (2015).
16. Di Fiore, B., Davey, N. E., Hagting, A., Izawa, D., Mansfeld, J., Gibson, T. J. & Pines, J. The ABBA Motif Binds APC/C Activators and Is Shared by APC/C Substrates and Regulators. *Dev. Cell* **32**, 358–372 (2015).
17. Ciossani, G., Overlack, K., Petrovic, A., Huis in 't Veld, P. J., Koerner, C., Wohlgemuth, S., Maffini, S. & Musacchio, A. The kinetochore proteins CENP-E and CENP-F directly and specifically interact with distinct BUB mitotic checkpoint Ser/Thr kinases. *J. Biol. Chem.* **293**, 10084–10101 (2018).
18. Bolanos-Garcia, V. M. & Blundell, T. L. BUB1 and BUBR1: multifaceted kinases of the cell cycle. *Trends Biochem. Sci.* **36**, 141–150 (2011).
19. Elowe, S. Bub1 and BubR1: at the Interface between Chromosome Attachment and the Spindle Checkpoint. *Mol. Cell. Biol.* **31**, 3085–3093 (2011).
20. Funabiki, H. & Wynne, D. J. Making an effective switch at the kinetochore by phosphorylation and dephosphorylation. *Chromosoma* **122**, 135–158 (2013).
21. Baron, A. P., von Schubert, C., Cubizolles, F., Siemeister, G., Hitchcock, M., Mengel, A., Schröder, J., Fernández-Montalván, A., von Nussbaum, F., Mumberg, D. & Nigg, E. A. Probing the catalytic functions of Bub1 kinase using the small molecule inhibitors BAY-320 and BAY-524. *eLife* **5**, e12187 (2016).
22. Zhang, G., Kruse, T., Guasch Boldú, C., Garvanska, D. H., Coscia, F., Mann, M., Barisic, M. & Nilsson, J. Efficient mitotic checkpoint signaling depends on integrated activities of Bub1 and the RZZ complex. *EMBO J.* **38**, (2019).
23. Gaudet, E. A., Huang, K.-S., Zhang, Y., Huang, W., Mark, D. & Sportsman, J. R. A Homogeneous Fluorescence Polarization Assay Adaptable for a Range of Protein Serine/Threonine and Tyrosine Kinases. *J. Biomol. Screen.* **8**, 164–175 (2003).
24. Mayr, L. M. & Bojanic, D. Novel trends in high-throughput screening. *Curr. Opin. Pharmacol.* **9**, 580–588 (2009).
25. Cronk, D. Chapter 8 - High-throughput screening. in *Drug Discovery and Development (Second Edition)* (eds. Hill, R. & Rang, H.) 95–117 (Churchill Livingstone, 2013).
26. Hall, M. D., Yasgar, A., Peryea, T., Braisted, J. C., Jadhav, A., Simeonov, A. & Coussens, N. P. Fluorescence polarization assays in high-throughput screening and drug discovery: a review. *Methods Appl. Fluoresc.* **4**, 022001 (2016).
27. Jameson, D. M. & Ross, J. A. Fluorescence Polarization/Anisotropy in Diagnostics and Imaging. *Chem. Rev.* **110**, 2685–2708 (2010).

28. Wermuth, C. G. Selective optimization of side activities: the SOSA approach. *Drug Discov. Today* **11**, 160–164 (2006).
29. Kirsch, P., Hartman, A. M., Hirsch, A. K. H. & Empting, M. Concepts and Core Principles of Fragment-Based Drug Design. *Molecules* **24**, 4309 (2019).
30. Gimeno, A., Ojeda-Montes, M., Tomás-Hernández, S., Cereto-Massagué, A., Beltrán-Debón, R., Mulero, M., Pujadas, G. & Garcia-Vallvé, S. The Light and Dark Sides of Virtual Screening: What Is There to Know? *Int. J. Mol. Sci.* **20**, 1375 (2019).
31. Hopkins, A. L., Keserü, G. M., Leeson, P. D., Rees, D. C. & Reynolds, C. H. The role of ligand efficiency metrics in drug discovery. *Nat. Rev. Drug Discov.* **13**, 105–121 (2014).
32. Bleicher, K. H., Böhm, H.-J., Müller, K. & Alanine, A. I. Hit and lead generation: beyond high-throughput screening. *Nat. Rev. Drug Discov.* **2**, 369–378 (2003).
33. Zhang, J.-H., Chung, T. D. Y. & Oldenburg, K. R. A Simple Statistical Parameter for Use in Evaluation and Validation of High Throughput Screening Assays. *J. Biomol. Screen.* **4**, 67–73 (1999).
34. Brideau, C., Gunter, B., Pikounis, B. & Liaw, A. Improved Statistical Methods for Hit Selection in High-Throughput Screening. *J. Biomol. Screen.* **8**, 634–647 (2003).
35. Howard, S., Berdini, V., Boulstridge, J. A., Carr, M. G., Cross, D. M., Curry, J., Devine, L. A., Early, T. R., Fazal, L., Gill, A. L., Heathcote, M., Maman, S., Matthews, J. E., McMenamin, R. L., Navarro, E. F., O'Brien, M. A., O'Reilly, M., Rees, D. C., Reule, M., Tisi, D., Williams, G., Vinković, M. & Wyatt, P. G. Fragment-Based Discovery of the Pyrazol-4-yl Urea (AT9283), a Multitargeted Kinase Inhibitor with Potent Aurora Kinase Activity. *J. Med. Chem.* **52**, 379–388 (2009).
36. Wang, S., Midgley, C. A., Scaërou, F., Grabarek, J. B., Griffiths, G., Jackson, W., Kontopidis, G., McClue, S. J., McInnes, C., Meades, C., Mezna, M., Plater, A., Stuart, I., Thomas, M. P., Wood, G., Clarke, R. G., Blake, D. G., Zheleva, D. I., Lane, D. P., Jackson, R. C., Glover, D. M. & Fischer, P. M. Discovery of *N* -Phenyl-4-(thiazol-5-yl)pyrimidin-2-amine Aurora Kinase Inhibitors. *J. Med. Chem.* **53**, 4367–4378 (2010).
37. Ling, J., Johnson, K. A., Miao, Z., Rakhit, A., Pantze, M. P., Hamilton, M., Lum, B. L. & Prakash, C. Metabolism and excretion of erlotinib, a small molecule inhibitor of epidermal growth factor receptor tyrosine kinase, in healthy male volunteers. *Drug Metab. Dispos.* **34**, 420–426 (2006).
38. Apsel, B., Blair, J. A., Gonzalez, B., Nazif, T. M., Feldman, M. E., Aizenstein, B., Hoffman, R., Williams, R. L., Shokat, K. M. & Knight, Z. A. Targeted polypharmacology: discovery of dual inhibitors of tyrosine and phosphoinositide kinases. *Nat. Chem. Biol.* **4**, 691–699 (2008).
39. Blasina, A., Hallin, J., Chen, E., Arango, M. E., Kraynov, E., Register, J., Grant, S., Ninkovic, S., Chen, P., Nichols, T., O'Connor, P. & Anderes, K. Breaching the DNA damage checkpoint via PF-00477736, a novel small-molecule inhibitor of checkpoint kinase 1. *Mol. Cancer Ther.* **7**, 2394–2404 (2008).
40. Ninkovic, S., Bennett, M. J., Rui, E. Y., Wang, F., Benedict, S. P., Teng, M., Wang, Y. & Zhu, J. Diazepinoindole derivatives as kinase inhibitors. WO2004063198A1 (2004).
41. Mader, M., de Dios, A., Shih, C., Bonjouklian, R., Li, T., White, W., de Uralde, B. L., Sánchez-Martinez, C., del Prado, M., Jaramillo, C., de Diego, E., Martín Cabrejas, L. M., Dominguez, C., Montero, C., Shepherd, T., Dally, R., Toth, J. E., Chatterjee, A., Pleite, S., Blanco-Urgoiti, J., Perez, L., Barberis, M., Lorite, M. J., Jambrina, E., Nevill, C. R., Lee, P. A., Schultz, R. C., Wolos, J. A., Li, L. C., Campbell, R. M. & Anderson, B. D. Imidazolyl benzimidazoles and imidazo[4,5-b]pyridines as potent p38α MAP kinase inhibitors with excellent in vivo antiinflammatory properties. *Bioorg. Med. Chem. Lett.* **18**, 179–183 (2008).
42. Pardanani, A., Lasho, T., Smith, G., Burns, C. J., Fantino, E. & Tefferi, A. CYT387, a selective JAK1/JAK2 inhibitor: in vitro assessment of kinase selectivity and preclinical studies using cell lines and primary cells from polycythemia vera patients. *Leukemia* **23**, 1441–1445 (2009).
43. Burns, C. J., Donohue, A. C., Feutrill, J. T., Nguyen, T. L. T., Wilks, A. F. & Zeng, J. Phenyl amino pyrimidine compounds and uses thereof. WO2008109943A1 (2008).
44. Moyer, J. D., Barbacci, E. G., Iwata, K. K., Arnold, L., Boman, B., Cunningham, A., DiOrio, C., Doty, J., Morin, M. J., Moyer, M. P., Neveu, M., Pollack, V. A., Pustilnik, L. R., Reynolds, M. M., Sloan, D., Theleman, A. & Miller, P. Induction of Apoptosis and Cell Cycle Arrest by CP-358,774, an Inhibitor of Epidermal Growth Factor Receptor Tyrosine Kinase. *Cancer Res.* **57**, 4838–4848 (1997).
45. Schnur, R. C. & Arnold, L. D. Quinazoline derivatives. WO1996030347A1 (1996).
46. Dotzauer, B., Grünert, R., Bednarski, P. J., Lanig, H., Landwehr, J. & Troschütz, R. 2,4-Diamino-9H-pyrimido[4,5-b]indol-5-ols: Synthesis, in vitro cytotoxic activity, and QSAR investigations. *Bioorg. Med. Chem.* **14**, 7282–7292 (2006).
47. Sato, H., Inoue, T., Ly, T.-W., Muramatsu, A., Shimazaki, M., Urbahns, K., Gantner, F., Okigami, H., Bacon, K. B., Komura, H., Yoshida, N. & Tsuno, N. 4-phenyl-pyrimido [4,5-b] indole derivatives. WO2004058764A1 (2004).
48. Stauffer, F., Maira, S.-M., Furet, P. & García-Echeverría, C. Imidazo[4,5-c]quinolines as inhibitors of the PI3K/PKB-pathway. *Bioorg. Med. Chem. Lett.* **18**, 1027–1030 (2008).
49. Anderson, M., Andrews, D. M., Barker, A. J., Brassington, C. A., Breed, J., Byth, K. F., Culshaw, J. D., Finlay, M. R. V., Fisher, E., McMiken, H. H. J., Green, C. P., Heaton, D. W., Nash, I. A., Newcombe, N. J., Oakes, S. E., Pauptit, R. A., Roberts, A., Stanway, J. J., Thomas, A. P., Tucker, J. A., Walker, M. & Weir, H. M. Imidazoles: SAR and development of a potent class of cyclin-dependent kinase inhibitors. *Bioorg. Med. Chem. Lett.* **18**, 5487–5492 (2008).

50. Rainey, M. D., Charlton, M. E., Stanton, R. V. & Kastan, M. B. Transient Inhibition of ATM Kinase Is Sufficient to Enhance Cellular Sensitivity to Ionizing Radiation. *Cancer Res.* **68**, 7466–7474 (2008).
51. Min, J., Guo, K., Suryadevara, P. K., Zhu, F., Holbrook, G., Chen, Y., Feau, C., Young, B. M., Lemoff, A., Connelly, M. C., Kastan, M. B. & Guy, R. K. Optimization of a Novel Series of Ataxia-Telangiectasia Mutated Kinase Inhibitors as Potential Radiosensitizing Agents. *J. Med. Chem.* **59**, 559–577 (2016).
52. Dugar, S., Chakravarty, S., Murphy, A., Mcenroe, G., Conte, A. & Perumattam, J. J. Quinazoline derivatives as medicaments. WO2005032481A2 (2005).
53. Foloppe, N., Fisher, L. M., Howes, R., Kierstan, P., Potter, A., Robertson, A. G. S. & Surgenor, A. E. Structure-Based Design of Novel Chk1 Inhibitors: Insights into Hydrogen Bonding and Protein−Ligand Affinity. *J. Med. Chem.* **48**, 4332–4345 (2005).
54. Walton, K. M., Fisher, K., Rubitski, D., Marconi, M., Meng, Q.-J., Sládek, M., Adams, J., Bass, M., Chandrasekaran, R., Butler, T., Griffor, M., Rajamohan, F., Serpa, M., Chen, Y., Claffey, M., Hastings, M., Loudon, A., Maywood, E., Ohren, J., Doran, A. & Wager, T. T. Selective Inhibition of Casein Kinase 1ϵ Minimally Alters Circadian Clock Period. *J. Pharmacol. Exp. Ther.* **330**, 430–439 (2009).
55. Chen, S., Zhang, Q., Wu, X., Schultz, P. G. & Ding, S. Dedifferentiation of Lineage-Committed Cells by a Small Molecule. *J. Am. Chem. Soc.* **126**, 410–411 (2004).
56. Ding, S., Wu, T. Y. H., Brinker, A., Peters, E. C., Hur, W., Gray, N. S. & Schultz, P. G. Synthetic small molecules that control stem cell fate. *Proc. Natl. Acad. Sci.* **100**, 7632–7637 (2003).
57. Ding, S., WU, T.-H., Gray, N. S. & Schultz, P. G. Compounds that induce neuronal differentiation in embryonic stem cells. WO2004093812A2 (2004).
58. Pierre, F., Chua, P. C., O'Brien, S. E., Siddiqui-Jain, A., Bourbon, P., Haddach, M., Michaux, J., Nagasawa, J., Schwaebe, M. K., Stefan, E., Vialettes, A., Whitten, J. P., Chen, T. K., Darjania, L., Stansfield, R., Anderes, K., Bliesath, J., Drygin, D., Ho, C., Omori, M., Proffitt, C., Streiner, N., Trent, K., Rice, W. G. & Ryckman, D. M. Discovery and SAR of 5-(3-Chlorophenylamino)benzo[*c*][2,6]naphthyridine-8-carboxylic Acid (CX-4945), the First Clinical Stage Inhibitor of Protein Kinase CK2 for the Treatment of Cancer. *J. Med. Chem.* **54**, 635–654 (2011).
59. Hu-Lowe, D. D., Zou, H. Y., Grazzini, M. L., Hallin, M. E., Wickman, G. R., Amundson, K., Chen, J. H., Rewolinski, D. A., Yamazaki, S., Wu, E. Y., McTigue, M. A., Murray, B. W., Kania, R. S., O'Connor, P., Shalinsky, D. R. & Bender, S. L. Nonclinical Antiangiogenesis and Antitumor Activities of Axitinib (AG-013736), an Oral, Potent, and Selective Inhibitor of Vascular Endothelial Growth Factor Receptor Tyrosine Kinases 1, 2, 3. *Clin. Cancer Res.* **14**, 7272–7283 (2008).
60. Kania, R. S., Bender, S. L., Borchardt, A. J., Cripps, S. J., Hua, Y., Johnson, M. D., Jr, T. O. J., Luu, H. T., Palmer, C. L., Reich, S. H., Tempczyk-Russell, A. M., Teng, M., Thomas, C., Varney, M. D., Wallace, M. B. & Collins, M. R. Indazole compounds and pharmaceutical compositions for inhibiting protein kinases, and methods for their use. US6534524B1 (2003).
61. Cheng, Y.-C. & Prusoff, W. H. Relationship between the inhibition constant (KI) and the concentration of inhibitor which causes 50 per cent inhibition (I50) of an enzymatic reaction. *Biochem. Pharmacol.* **22**, 3099–3108 (1973).
62. Young, R. J. & Leeson, P. D. Mapping the Efficiency and Physicochemical Trajectories of Successful Optimizations. *J. Med. Chem.* **61**, 6421–6467 (2018).
63. Ninkovic, S. & Rynberg, R. Polymorphic forms of (2r,z)-2-amino-2-cyclohexyl-n-(5-(1-methyl-1h-pyrazol-4ʊl)-1-oxo-2,6-dihydro-1h-[1,2]diazepino[4,5,6-cd]indol-8-yl)acetamide. WO2007113647A1 (2007).
64. Olesen, S. H., Zhu, J.-Y., Martin, M. P. & Schönbrunn, E. Discovery of Diverse Small-Molecule Inhibitors of Mammalian Sterile20-like Kinase 3 (MST3). *ChemMedChem* **11**, 1137–1144 (2016).
65. Stamos, J., Sliwkowski, M. X. & Eigenbrot, C. Structure of the Epidermal Growth Factor Receptor Kinase Domain Alone and in Complex with a 4-Anilinoquinazoline Inhibitor. *J. Biol. Chem.* **277**, 46265–46272 (2002).
66. Foran, J., Ravandi, F., Wierda, W., Garcia-Manero, G., Verstovsek, S., Kadia, T., Burger, J., Yule, M., Langford, G., Lyons, J., Ayrton, J., Lock, V., Borthakur, G., Cortes, J. & Kantarjian, H. A Phase I and Pharmacodynamic Study of AT9283, a Small-Molecule Inhibitor of Aurora Kinases in Patients With Relapsed/Refractory Leukemia or Myelofibrosis. *Clin. Lymphoma Myeloma Leuk.* **14**, 223–230 (2014).
67. Dent, S. F., Gelmon, K. A., Chi, K. N., Jonker, D. J., Wainman, N., Capier, C. A., Chen, E. X., Lyons, J. F. & Seymour, L. NCIC CTG IND.181: Phase I study of AT9283 given as a weekly 24 hour infusion in advanced malignancies. *Invest. New Drugs* **31**, 1522–1529 (2013).
68. Arkenau, H.-T., Plummer, R., Molife, L. R., Olmos, D., Yap, T. A., Squires, M., Lewis, S., Lock, V., Yule, M., Lyons, J., Calvert, H. & Judson, I. A phase I dose escalation study of AT9283, a small molecule inhibitor of aurora kinases, in patients with advanced solid malignancies. *Ann. Oncol.* **23**, 1307–1313 (2012).
69. Moreno, L., Marshall, L. V., Pearson, A. D. J., Morland, B., Elliott, M., Campbell-Hewson, Q., Makin, G., Halford, S. E. R., Acton, G., Ross, P., Kazmi-Stokes, S., Lock, V., Rodriguez, A., Lyons, J. F., Boddy, A. V., Griffin, M. J., Yule, M. & Hargrave, D. A Phase I Trial of AT9283 (a Selective Inhibitor of Aurora Kinases) in Children and Adolescents with Solid Tumors: A Cancer Research UK Study. *Clin. Cancer Res.* **21**, 267–273 (2015).
70. Cyclacel Pharmaceuticals, Inc. A Phase I Pharmacologic Study of CYC116, an Oral Aurora Kinase Inhibitor, in Patients With Advanced Solid Tumors. Identifier: NCT00560716, https://clinicaltrials.gov/ct2/show/NCT00560716 (Accessed 5 July 2021) (2007).

71. Wang, S., Meades, C., Wood, G., Osnowski, A., Anderson, S., Yuill, R., Thomas, M., Mezna, M., Jackson, W., Midgley, C., Griffiths, G., Fleming, I., Green, S., McNae, I., Wu, S.-Y., McInnes, C., Zheleva, D., Walkinshaw, M. D. & Fischer, P. M. 2-Anilino-4-(thiazol-5-yl)pyrimidine CDK Inhibitors: Synthesis, SAR Analysis, X-ray Crystallography, and Biological Activity. *J. Med. Chem.* **47**, 1662–1675 (2004).
72. Masse, C. E. Substituted oxazolidinone derivatives. WO2009023233A1 (2009).
73. Kompella, A., Adibhatla, B. R. K., Muddasani, P. R., Rachakonda, S., Gampa, V. K. & Dubey, P. K. A Facile Total Synthesis for Large-Scale Production of Imatinib Base. *Org. Process Res. Dev.* **16**, 1794–1804 (2012).
74. Dowell, J., Minna, J. D. & Kirkpatrick, P. Erlotinib hydrochloride. *Nat. Rev. Drug Discov.* **4**, 13–14 (2005).
75. Zhang, Y., Ding, K., Liao, J., Wang, Y. & Chen, P. Coupling compounds of nsaid anti-inflammatory and analgesic drugs and egfr kinase inhibitors, synthesis methods and applications thereof. US20160175453A1 (2016).
76. Wang, X., Ju, T., Li, X. & Cao, X. Regioselective Alkylation of Catechols via Mitsunobu Reactions. *Synlett* **2010**, 2947–2949 (2010).
77. Gregson, S. J., Howard, P. W., Gullick, D. R., Hamaguchi, A., Corcoran, K. E., Brooks, N. A., Hartley, J. A., Jenkins, T. C., Patel, S., Guille, M. J. & Thurston, D. E. Linker Length Modulates DNA Cross-Linking Reactivity and Cytotoxic Potency of C8/C8′ Ether-Linked C2- *exo* -Unsaturated Pyrrolo[2,1- *c*][1,4]benzodiazepine (PBD) Dimers. *J. Med. Chem.* **47**, 1161–1174 (2004).
78. Knight, Z., Apsel, B. & Shokat, K. Kinase antagonists. US20070293516A1 (2007).
79. Dar, A. C. & Shokat, K. M. The Evolution of Protein Kinase Inhibitors from Antagonists to Agonists of Cellular Signaling. *Annu. Rev. Biochem.* **80**, 769–795 (2011).
80. Liao, J. J.-L. Molecular Recognition of Protein Kinase Binding Pockets for Design of Potent and Selective Kinase Inhibitors. *J. Med. Chem.* **50**, 409–424 (2007).
81. The PyMOL Molecular Graphics System, Version 2.3.0 Schrödinger, LLC.